Philipps-Universität Marburg

Johannes Gille

Fachbereich 17
AG Allgemeine und Biologische Psychologie
AE Theoretische Kognitionswissenschaft

Learning in cortical microcircuits with multi-compartment pyramidal neurons

Supervisors:

Prof. Dr. Dominik Endres, Philipps-Universität Marburg

Dr. Johan Kwisthout, Radboud University

Contents

Chapter 1

Introduction

1.1   Motivation

TODO: fill with citations?

The outstanding learning capabilities of the human brain have been found to be elusive and as of yet impossible to replicate in silicio. While the power and utility of classical Machine-learning solutions has improved greatly in recent years, these approaches can not serve as an adequate model of human cognition. The sheer number of neurons and synapses in the brain makes simulations of an entire brain impossible with current hardware constraints. In fact, it has been found to be a substantial challenging to create artificial neural networks that simulate even parts of human neurophysiology while simultaneously being able to learn in a goal-oriented way.

The literature entails numerous approaches to adress these challenges, with varying degrees of success. In this thesis, I will investigate one such approach, and attempt to modify it in a way that it more closely resembles properties exhibited by the human neocortex.

1.2   The Backpropagation of errors algorithm

The Backpropagation of errors algorithm (*Backprop*) forms the backbone of modern machine learning and is able to outperform humans on some tasks **TODO: cite**. Particularly for training deep neural networks it has remained a popular choice since its initial development. Its power for supervised learning stems from to its unique capability to attribute errors in the output of a network to activations of specific neurons within its hidden layers. This property also forms the basis of the algorithm's name; After an initial forward pass to form a prediction about the nature of a given input, a separate backward pass propagates the arising error through all layers in reverse order. During this second network traversal, local error gradients dictate to what extent a given weight needs to be altered so that the next presentation of the same sample would elicit a lower error in the output layer.

While Backprop continues to prove exceptionally useful in conventional machine learning systems, it is viewed critically by many neuroscientists. For one, Backprop relies on a slow adaptation of synaptic weights, and therefore requires a large amount of examples to learn rather simple input-output mappings. In this way, its performance is far inferior to the powerful one-shot learning exhibited by humans (Brea and Gerstner, 2016). Yet more importantly, no plausible mechanisms have yet been found by which biological neural networks could implement this algorithm. In fact, Backprop as an algorithm by which brains may learn has been dismissed entirely by much of the neuroscience community for decades (Grossberg, 1987; Crick, 1989; Mazzoni et al., 1991; O'Reilly, 1996). This dismissal is often focussed on three mechanisms that are instrumental for the algorithm (Whittington and Bogacz, 2019; Bengio et al., 2015; Liao et al., 2016):

1.2.1 Local error representation

Neuron-specific errors in Backprop are computed and propagated by a mechanism that is completely detached from the network itself, which requires access to the entirety of the network state. In order to compute the weight changes for a given layer, the algorithm takes as an input the activation and synaptic weights of all downstream neurons. In contrast, plasticity in biological neurons is largely considered to be primarily dependent on factors that are local to the synapse (Abbott and Nelson, 2000; Magee and Grienberger, 2020; Urbanczik and Senn, 2014). While neuromodulators are known to influence synaptic plasticity, their dispersion is too wide to communicate neuron-specific errors**TODO: cite**. Thus, biologically plausible Backprop would require a method for encoding local errors locally, i.e. close to the neurons which cause them. This has been perhaps the strongest criticism of Backprop in the brain, as both qestions about the mechanisms for computing and storing these errors remain unanswered as of yet.

1.2.2 The weight transport problem

During the weight update stage of Backprop, errors are transmitted between layers with the same weights that are used in the forward pass. In other words, the magnitude of a neuron-specific error that is propagated through a given connection should be proportional to its impact on output loss during the forward pass. For this to work, a neuronal network would require feedback connections that mirror both the network structure and synaptic weights exhibited by the original network. It was long assumed that the feedback weights are required to be an exact match, but (Liao et al., 2016) showed, that this constraint can be relaxed somewhat to a concordance of weight signs.

Bidirectional connections are common in the cortex, yet it is unclear by which mechanism pairs of synapses would be able to align. This issue becomes particularly apparent when considering long-range pyramidal projections, in which feedforward and feedback synapses

would potentially be separated by a considerable distance.

1.2.3 Neuron models

Finally, the types of artificial neurons typically used in Backprop transmit a continuous scalar activation at all times, instead of discrete spikes. In theory, these activations correspond to the firing rate of a spiking neuron, giving this class of models the title *rate neurons*. Yet particularly with regard to synaptic plasticity, spike based communication often requires completely novel approaches. Plasticity rules in rate neurons do not necessarily have an easily derived counterpart for spiking neurons. A notable example for this issue is Backprop itself; The local error gradient $\frac{\delta E}{\delta \phi(u_i)}$ of a neuron i is not trivial to compute for Spiking neural networks (SNN), as a spiketrain has no natural derivative. Furthermore, a given neuron's activation in classical Backprop is computed from a simple weighted sum of all inputs. This fails to capture the complex nonlinearities of dendritic integration that are fundamental to cortical neurons (Gerstner and Naud, 2009; Sjostrom et al., 2008; Eyal et al., 2018). Finally, these abstract neurons - at least in classical Backprop - have no persistence through time. Thus, their activation is dictated strictly by the presentation of a single stimulus, in contrast to the leaky membrane dynamics exhibited by biological neurons.

Additional concerns regarding Backprop will be discussed in Section **TODO:** .

1.3 Alternatives to classical Backprop

The complexity of the algorithm has led neuroscience to largely dismiss Backprop as a plausible learning mechanism for biological brains. Yet, Backprop has remained the gold standard against which all supervised learning mechanisms eventually have to compare, as it is unmatched in learning performance for many tasks. Also, despite its apparent biological implausibility, it does share some notable parallels to learning in the brain: When training on real-world data, artificial neural networks have been shown to learn similar representations as those found in brain areas responsible for comparable tasks McClelland et al. (1995); **?**); Yamins and DiCarlo (2016). Thus, several attempts have been made to define more biologically plausible learning rules which are able to approach the performance of Backprop. A full review of the available literature would be out of scope for this thesis, so only a few examples will be discussed in this section.

One approach to solve the issues around local error representations is, to drive synaptic plasticity through a global error signal. The appeal of this solution is that this task could be plausibly performed by neuromodulators like Dopamine (Mazzoni et al., 1991; Seung, 2003; Izhikevich, 2007). While these solutions enable a kind of reinforcement learning, performance of global error/reward signalling stays far behind that of the exact credit assignment performed

	Temporal-error model		Explicit-error model	
	Contrastive learning	Continuous update	Predictive coding	Dendritic error
Control signal	Required	Required	Not required	Not required
Connectivity	Unconstrained	Unconstrained	Constrained	Constrained
Propagation time	L-1	L-1	2L-1	L-1
Pre-training	Not required	Not required	Not required	Required
Error encoded in	Difference in activity between separate phases	Rate of change of activity	Activity of specialised neurons	Apical dendrites of pyramidal neurons
Data accounted for	Neural responses and behaviour in a variety of tasks	Typical spike-time-dependent plasticity	Increased neural activity to unpredicted stimuli	Properties of pyramidal neurons
MNIST performance	~2-3	-	~1.7	~1.96

Table 1.1: Comparison between some leading biologically plausible approximations of Backprop, adapted from Whittington and Bogacz (2019). From left to right: Contrastive hebbian learning (O'Reilly, 1996), Contrastive learing with continuous update (Bengio et al., 2017), Predictive Coding (Whittington and Bogacz, 2017; Rao and Ballard, 1999), Dendritic error network (Sacramento et al., 2018). All algorithms were selected due to them reflecting some properties of biological brains, some of which are highlighted in the row "Data accounted for". To do this, all of them need to make concessions. In the first few rows, desirable properties are highlighted in green, while undesirable traits are highlighted in red.

in Backprop. Additionally, this class of algorithms requires even more examples of a pattern, and was shown to scale poorly with network size (Werfel et al., 2003).

The weight transport problem was similarly adressed through a mechanism called *Feedback Alignment* Lillicrap et al. (2014). This seminal paper shows that Backpropagation of errors can still be successful when feedback weights are random. In addition to learning an input-output mapping, Backpropagation is capable of training a network to gain information from randomly weighted instructive pathways. The authors call this process *learning to learn*.

1.4 Cortical microcircuits

Chapter 2

Methods

2.1 Neuron and network model

This section will go into detail about the dendritic error network (Sacramento et al., 2018). The model contains a somewhat complex and strongly recurrent connectivity, which poses one of the major criticisms aimed at it (Whittington and Bogacz, 2019). Much like traditional machine learning networks, it can be functionally separated into layers. Yet in this particular model, input- hidden- and output layers are quite distinct in both neuron populations and connectivity.

2.1.1 Network architecture

The basic connectivity scheme of the Model is shown in Figure 2.1. Neurons at the input layer receive no feedback signals and serve primarily to apply a temporals low-pass filter to the stimulus which is injected directly into their membrane. Hidden layers consist of a pyramidal- and an interneuron population, which are fully connected to each other reciprocally. Both types of neurons are represented by multi-compartment neuron models with leaky membrane dynamics. Interneurons contain one somatic and one dendritic compartment, while pyramidal neurons are modeled with both a basal and an apical dendrite (cf. Section 2.1.2). Feedforward connections between layers are facilitated by all-to-all connections between their respective pyramidal neurons and innervate basal compartments. Hidden layer pyramidal neurons additionally connect to all interneurons within their layer. Feedback connections from superficial pyramidal neurons and lateral interneurons on the other hand arrive at apical compartments of pyramidal neurons. Thus, a hidden layer pyramidal neuron forms two reciprocal loops, one with all interneurons in the same layer, and one with all pyramidal neurons in the next layer.

Hidden layer interneurons receive feedback information from superficial pyramidal neurons in addition to their lateral connections. These feedback connections are special, since they

---

[1]Note that the input layer is displayed as having interneurons here. This appears to be a mistake in the Figure. Within the implementation, interneurons are only modelled in hidden layers.
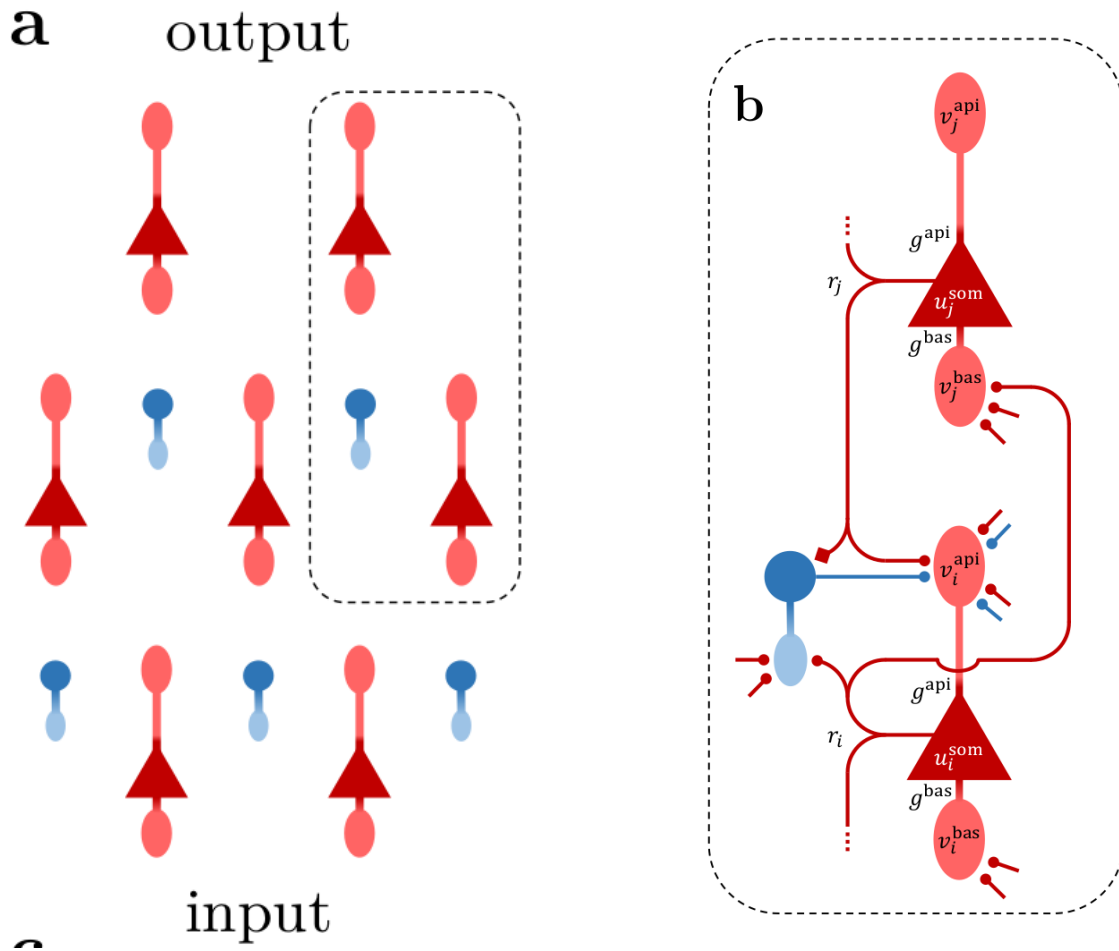
Figure 2.1: Network structure, from Haider et al. (2021). **a:** pyramidal- (red) and interneurons (blue) in a network of three layers. Note the fact that the number interneurons in a layer is equal to the number of pyramidal neurons in the subsequent layer[1]. **b:** connectivity within the highlighted section. Feedback pyramidal-to-interneuron connections (displayed with rectangular synapse) transmit pyramidal somatic potential directly and connect to a single interneuron. This enables these interneurons to learn to match their corresponding next-layer pyramidal neurons. All other synapses (circles) transmit the neuron somatic activation $\phi(u^{som})$ and fully connect their origin and target populations.

connect one pyramidal neuron to exactly one interneuron. Instead of transmitting a neuronal activation $\phi(u^P_{l+1})$ as all other connections do, these connections relay somatic voltage u^P_{l+1} directly. This one-to-one connectivity puts a strict constraint on the number of interneurons in a hidden layer, as it must match the number of subsequent pyramidal neurons. These pairs of inter- and pyramidal neurons that have matching somatic activations will henceforth be called *sister neruons*. Their connections serve to *nudge* interneuron somatic activation towards that of their pyramidal sisters. The purpose of an interneuron in this architecture is then, to predict the activity of its sister neuron. Any failure to do so results in layer-specific errors which in turn are the driving force of learning in this context, but more on this later. The connectivity between them share features of electrical synapses, which will be discussed in Section 3.1. **TODO: keep last sentence?**

Output layers have no interneurons, and are usually modeled as pyramidal neurons without an apical compartment. During learning, the target for the network's activation is injected into their somatic compartment. Through the feedback connections, it can propagate through the entire network. To understand what purpose this rather complex connectivity scheme serves in our model, neuron models and plasticity rules require some elaboration.

2.1.2 Neuron models

The network contains two types of multi-compartment neurons; Pyramidal neurons with three compartments each, and interneurons with two compartments each. They integrate synaptic inputs into dendritic potentials, which in turn leak into the soma with specific conductances. Note that vector notation will be used throughout this section, and u_l^P and u_l^I denote the column vectors of pyramidal- and interneuron somatic voltages at layer l respectively. Synaptic weights W are likewise assumed matrices of size $n \times m$, which are the number of output and input neurons of the connected populations respectively. The activation r_l^P of pyramidal neurons is given by applying the synaptic transfer function ϕ to to their somatic potentials u_l^P:

$$r_l^P = \phi(u_l^P) \tag{2.1}$$

$$\phi(x) = \begin{cases} 0 & \text{if } x < -\varepsilon \\ \gamma \, log(1 + e^{\beta(x-\theta)}) & \text{if } -\varepsilon \le x < \varepsilon \\ \gamma \, x & \text{otherwise} \end{cases} \tag{2.2}$$

where ϕ acts componentwise on u and can be interpreted as a smoothed variant of ReLu (sometimes called *Softplus*) with scaling factors $\gamma = 1$, $\beta = 1$, $\theta = 0$. Splitting the computation with the threshold parameter $\varepsilon = 15$ does not change its output, but instead serves to prevent overflow errors for large absolute values of x.

As mentioned before, pyramidal and interneurons are modeled as rate neurons with leaky membrane dynamics and multiple compartments. Where applicable, they will be differentiated with superscripts P and I respectively. The derivative somatic membrane potentials of layer l pyramidal neurons is given by:

$$C_m \dot{u}_l^P = -g_l u_l^P + g^{bas} v_l^{bas} + g^{api} v_l^{api} \tag{2.3}$$

where g_l is the somatic leakage conductance, and C_m is the somatic membrane capacitance, which will be assumed to be 1 from here on out. v_l^{bas} and v_l^{api} are the membrane potentials of basal and apical dendrites respectively, and g^{bas} and g^{api} their corresponding coupling conductances. Dendritic compartments in this model have no persistence between simulation steps. Thus, they are defined at every timestep t through incoming weight matrices and presynaptic activities:

$$v_l^{bas}(t) = W_l^{up} \; \phi(u_{l-1}^P(t)) \tag{2.4}$$

$$v_l^{api}(t) = W_l^{pi} \; \phi(u_l^I(t)) \; + \; W_l^{down} \; \phi(u_{l+1}^P(t)) \tag{2.5}$$

The nomenclature for weight matrices conforms to Haider et al. (2021), where weight matrices are indexed by the layer in which their neurons terminate and belong to one of four populations: Feedforward and feedback pyramidal-to-pyramidal connections arriving at layer l are denoted W_l^{up} and W_l^{down} respectively. Lateral pyramidal-to-interneuron connections are denoted with W_l^{ip} and their corresponding feedback connections with W_l^{pi}. Since the input layer contains no synapses, indexing begins with 0 for the first hidden layer.

Interneurons integrate synaptic information by largely the same principle, but instead of the signals from sister neurons arriving at an apical compartment, it is injected directly into the soma. Through this, interneurons functionally resemble the original two-compartment neuron from Urbanczik and Senn (2014) most closely.

$$C_m \dot{u}_l^I = -g_l u_l^I + g^{dend} v_l^{dend} + i^{nudge,I} \tag{2.6}$$

$$i^{nudge,I} = g^{nudge,I} u_{l+1}^P \tag{2.7}$$

$$v_l^{dend} = W_l^{ip} \; \phi(u_l^P) \tag{2.8}$$

where $g^{nudge,I}$ is the interneuron nudging conductance, and u_{l+1}^P is the somatic voltage of pyramidal neurons in the next layer. Pyramidal neurons in the output layer N effectively behave like interneurons, as they receive no input to their apical compartment. Instead, the target activation u^{tgt} is injected into their soma:

$$C_m \dot{u}_N^P = -g_l u_N^P + g^{bas} v_N^{bas} + i^{nudge,tgt} \tag{2.9}$$

$$i^{nudge,tgt} = g^{nudge,tgt} u^{tgt} \tag{2.10}$$

These neuron dynamics correspond closely to those by Urbanczik and Senn (2014), including the extension to more than two compartments which was proposed in the original paper. It should be noted however, that they are simplified in some ways. For example, dendritic couplings and nudging are not relative to the somatic or some reversal potential (i.e. $i^{nudge,tgt} = g^{nudge,tgt}(u^{tgt} - u_N^P)$), but are only dependent on absolute currents. Additionally, the strict separation of excitatory and inhibitory synaptic integration (cf. Section **TODO: write about this**), as well as additional nonlinearities in the plasticity are omitted. These simplifications do increase computational speed and allow for a much simpler approximation of

network dynamics via a steady-state. Yet they do come at the cost of omitting neuroscientific insights from the model, which I view critically. **phrasing**

2.2 Urbanczik-Senn Plasticity

The synapses in the network are all modulated according to variations of the "Urbanczik-Senn" plasticity rule (Urbanczik and Senn, 2014), which will be discussed in this section. After detailing the (simplified) weight update, I will briefly discuss the scientific significance of the plasticity model.

2.2.1 Derivation

The plasticity rule is only defined for postsynaptic neurons which have one somatic and at least one dendritic compartment, to the latter of which synapses with this plasticity can connect. Functionally, synaptic weights are changed in such a way, as to minimize discrepancies between somatic and dendritic potential. This discrepancy is called the *dendritic error*. The change in weight for a synapse fron neuron j to the basal compartment of a pyramidal neuron i is given by:

$$\dot{w}_{ij} = \eta \ (\phi(u_i^{som}) - \phi(\hat{v}_i^{bas})) \ \phi(u_j^{som})^T \tag{2.11}$$

$$\hat{v}_i^{bas} = \alpha \ v_i^{bas} \tag{2.12}$$

with learning rate η, and u^T denoting the transposition of the vector u (which is by default assumed a column vector). The dendritic prediction $\hat{v}_i^{bas}$ is a scaled version of the dendritic potential by the constant factor α, which is calculated from coupling and leakage conductances. As an example, basal dendrites of pyramidal neurons in Sacramento et al. (2018) are attenuated by $\alpha = \frac{g^{bas}}{g_l + g^{bas} + g^{api}}$. A key property of this value for α is, that dendritic error is 0, when the only input to a neuron stems from the given dendrite. In other words, the dendrite predicts somatic activity perfectly. Neuron- and layer-specific differences in α, as well as an analytical derivation are detailed in (Sacramento et al., 2018).

If a current is injected into the soma (or in this case, into a different dendrite), a dendritic error arises, and plasticity drives synaptic weights to minimize it. In addition to the learning rate η, $\dot{w}_{ij}$ scaled by the presynaptic activity $\phi(u_j^{som})$. Therefore, a dendritic error arising without presynaptic contribution does not elicit a change in that particular synapse. Updates for the weight matrices in a hidden layer l of the present network model are given by:

$$\dot{w}_l^{up} = \eta_l^{up} \ (\phi(u_l^P) - \phi(\hat{v}_l^{bas})) \ \phi(u_{l-1}^P)^T \tag{2.13}$$

$$\dot{w}_l^{ip} = \eta_l^{ip} \ (\phi(u_l^I) - \phi(\hat{v}_l^{dend})) \ \phi(u_l^P)^T \tag{2.14}$$

$$\dot{w}_l^{pi} = \eta_l^{pi} \ - v_l^{api} \ \phi(u_l^I)^T \tag{2.15}$$

$$\dot{w}_l^{down} = \eta_l^{down} \ (\phi(u_l^P) - \phi(w_l^{down} r_{l+1}^P)) \ \phi(u_{l+1}^P)^T \tag{2.16}$$

Each set of connections is updated with a specific learning rate η and a specific dendritic error term. The purpose of these error terms will be explained in Section 2.3. Note that pyramidal-to-pyramidal feedback weights w_l^{down} are not plastic in the present simulations and are only listed for completeness, see Section 5.4.

2.2.2 Neuroscientific significance

TODO: this is going to be hard

Dendritic plateau potentials

TODO: Dendritic spikes

2.3 The self-predicting network state

In this model, euron dynamics, plasticity rules and network architecture form an elegant interplay, which I expand on in this section. We will

Since each interneuron receives a somatic nudging signal from its corresponding next-layer pyramidal neuron, incoming synapses from lateral pyramidal neurons adapt their weights to match feedforward pyramidal-to-pyramidal weights. In intuitive terms; Feedforward pyramidal-to-pyramidal weights elicit a certain activation in the subsequent layer, which is fed back into corresponding interneurons. In order to minimize the dendritic error term in Equation 2.14, pyramidal-to-interneuron weight matrices at every layer must match these forward weights $(w_l^{ip} \approx \rho w_l^{up})$ up to some scaling factor ρ. ρ depends on the difference in parameters between pyramidal- and interneurons, and is close to 1 for most of the simulations considered here. As long as no feedback information arrives at the pyramidal neurons, the Urbanczik-Senn plasticity drives synaptic weight to fulfill this constraint. Note, that this alignment of two separate sets of outgoing weights is acheived with only local information. Therefore this mechanism could plausibly align the weights of biological synapses that are physically separated by long distances.

Next, consider the special case for interneuron-to-pyramidal weights in Equation 2.15, in which plasticity does not serve to reduce discrepancies between dendritic and somatic potential.

The error term is instead defined solely by the apical compartment voltage[2]. Thus, plasticity in these synapses works towards silencing the apical compartment. The apical compartments also receive feedback from superficial pyramidal neurons, whose synapses will be considered non-plastic for now. As shown above, interneurons each learn to match their respective sister neuron activity. Thus, silencing of apical compartments can only be acheived by mirroring the pyramidal-to-pyramidal feedback weights ($w_l^{pi} \approx -w_l^{down}$).

When enabling plasticity in only these two synapse types, the network converges on the "**self-predicting state**" (Sacramento et al., 2018). This state is defined by a minimization of four error metrics at each hidden layer l:

- The symmetries between feedforward ($w_l^{ip} \approx \rho w_l^{up}$) and feedback ($w_l^{pi} \approx -w_l^{down}$) weights. Mean squared error between these pairs of matrices will be called **Feedforward -** and **Feedback weight error** respectively.

- Silencing of pyramidal neuron apical compartments ($v_l^{api} \approx 0$). The Frobenius norm **TODO: cite** of apical compartment voltages within a layer is called the **Apical error**.

- Equal activations in interneurons and their respective sister neurons ($\phi(u_l^I) \approx \phi(u_{l+1}^P)$). The mean squared error over these vectors is called the **Interneuron error**.

is there a mathematical symbol for this type of convergence?

All of these equalities are approximate, since the network does not ever reach a state in which all of these values are zero. In the original implementation, these deviations are minute and can likely be explained with floating point conversions. Since it is impossible to replicate the timing of the original precisely within NEST, the NEST simulations deviate more strongly from this ideal. The key insight here is, that this state is not clearly defined by absolute error thresholds, but is rather flexible. Thus, networks are able to learn successfully even when their weights are initialized imperfectly. **TODO: or not at all? some science is required here**

An analysis of the equations describing the network reveals that the self-predicting state is stable **phrasing**. When Interneuron error is zero, dendritic and somatic compartments of all interneurons are equal, thus effectively disabling plasticity in incoming synapses. Likewise, a silenced apical compartment will disable plasticity in all incoming synapses. Synapses from lateral interneurons (Equation 2.15) only depend on the apical compartment itself, thus can not change in this state. Similarly, the apical compartment is also the driving factor for the dendritic error of feedforward synapses (Equation 2.13), since it affects somatic activity when active[3]. Thus, all plasticiy in the network is disabled, and remains in the self-predicting state

---

[2]In strict terms, it is defined by the deviation of the dendritic potential from its specific reversal potential. Since that potential is zero throughout, $-v_l^{api}$ remains as the error term.

[3]This feature is actually rather important when contemplating biological neurons using the Urbanczik-Senn plasticity. In the original paper, currents were injected directly into the soma to change the error term. The the introduction of a second dendrite which performs that very task is much more useful, as originally described

regardless of the kind of stimulus injected into the input layer. This fact highlights another important property of networks in this state. Notice, how information flows backwards through the network; All feedback signals between layers ultimately pass through the apical compartments of pyramidal neurons. Thus, successful silencing of all apical compartments implies that no information can travel backwards between layers (with the exception of interneurons receiving top down signals). As a result, the network behaves strictly like a fully connected feedforward network consisting only of pyramidal neurons. The recurrence within this network is in balance, and completely cancels out its own effects. This holds true as long as all conditions for the self-predicting state are fulfilled, and the network only receives external stimulation at the input layer. One interpretation of this is, that the network has learned to predict its own top-down input. A failure by interneurons to fully explain (i.e. cancel out) top-down input thus results in a prediction error, encoded in deviation of apical dendrite potentials from their resting state. This prediction error in turn elicits plasticity in all synapses connecting to its pyramidal neuron, which drives the network towards a self-predicting state that is congruent with the novel top-down signal. Therefore, these neuron- specific prediction errors are the driving force of supervised learning in these networks

2.4 Training the network

Starting with a network in the self-predicting state, performing time-continuous supervised learning then requires an injection of a target activation into the network's output layer alongside with a stimulus at the input layer. Since output layer neurons feed back into both interneurons and pyramidal neurons of the previous layer, local prediction errors arise. Synapses activatee and drive to minimize the prediction errors, which requires the network to replicate the target activation from activations and weights of the last hidden layer.

Note, that this mechanism is not exclusive to the last two layers. Any Apical errors cause a change in somatic activity, which previous layers will fail to predict. Thus, errors are propagated backwards through the entire network, causing error minimization at every layer. See the Supplementary analysis of Sacramento et al. (2018) for a rigorous proof that this type of network does indeed approximate the Backpropagation algorithm **what does the O mean?** .

Classical backpropagation relies on a strict separation of a forward pass of some stimulus, and subsequent a backwards pass dependent on the arising loss at the output layer. Since the present network is time-continuous, stimulus and target activation are injected into the network simultaneously. These injections are maintained for a given presentation time t_{pres}, in order to allow the network to calculate errors through its recurrent connections before slowly adapting weights. Particluarly for deep networks, signals travelling from both the input and

---

by the authors. Whether interneurons could be modeled by the same principles will be discussed in Section **TODO: talk about interneuron dendritic trees**

output layer require some time to balance out and elicit the correct dendritic error terms. This property poses the most significatn drawback of this type of time-continuous approximation of Backpropagation: The network tends to overshoot activations in some neurons, which in turn causes an imbalance between dendritic and somatic compartments. This effect causes the network to change synaptic weights away from the desired state during the first few miliseconds of a stimulus presentation. The solution Sacramento et al. found for this issue was to drastically reduce learning rates, while increasing stimulus presentation time. This solution is sufficient to prove that plasticity in this kind of network is able to perform error propagation, but still has some issues. Most notably, training is highly inefficient and computationally intensive. A closer investigation of the issue as well as a solution will be discussed in Section 2.8.

2.5   The NEST simulator

One of the key research questions motivating this thesis is whether the network would be able to learn successfully when employing spike-based communication instead of the rate neurons for which it was developed. As a framework for my spike-based implementation two options were considered: The first one was to use the existing implementation of the network which employs `PyTorch` and `NumPy`, and expand it to employ spiking neurons. PyTorch does in principle support spiking communication between layers, but is streamlined for implementing less recurrent and less complex network and neuron models. Another concern is efficiency; PyTorch is very well optimized for efficiently computing matrix operations on dedicated hardware. This makes it a good choice for simulating large networks of rate neurons, which transmit all of their activations between layers at every simulation step. Spiking communication between leaky neurons is almost antithetical to this design philosophy and thus can be expected to perform comparatively poor when using this backend.

The second option was to use the NEST simulator (nest-simulator.readthedocs.io), which was developed with highly parallel simulations of large spiking neural networks in mind. It is written in C++ and uses the *Message Passing Interface* (MPI) to efficiently communicate evends between both threads and compute nodes. One design pillar of the simulator, which is particularly relevant for this project, is the event-based communication scheme that underpins all simulated nodes. It ensures that communication bandwidth at every simulation step is only used by the subset of nodes which transmit spikes or other signals at that time step. Yet the most notable advantage of the NEST simulator is, that an event-based implementation of the Urbanczik-Senn plasticity alongside a corresponding neuron model had already been developed for it. Combined with the fact that I had more prior experience with NEST over PyTorch, I decided to implement the spiking neuron model in the NEST simulator.

The simulator has one particular limitation which needs to be considered. As communication between compute nodes takes time, Events[4] can not be handled in the same simulation

---

[4]An Event in NEST is an abstract C++ Class that is created by neurons, and transmitted across threads and

step in which they were sent. Thus, NEST enforces a synaptic transmission delay of at least one simulation step for all connections. This property is integral to many parallel simulation backends (Davies et al., 2018; Hines and Carnevale, 1997; de Schepper et al., 2022), and is in line with synaptic delays of biological neurons. Yet particularly with regard to network relaxation, it can be expected to affect performance.

2.6   Transitioning to spiking communication

The spiking neuron models rely heavily on the model from (Stapmanns et al., 2021), in which it was shown that spiking neurons are able to perform learning tasks that were designed for the rate neurons described in Urbanczik and Senn (2014). The existing model is an exact replication of the Urbanczik-Senn neuron in terms of membrane dynamics. The critical update of that model is that instead of transmitting their hypothetical rate $r = \phi(u)$ at every time step, these neurons emit spikes in a similar way to stochastic binary neurons (Ginzburg and Sompolinsky, 1994). The number of spikes to be generated during a simulation step n is determined by drawing from a Poisson distribution, which takes r as a parameter:

$$P\{n \text{ spikes during } \Delta t\} = e^{-r\Delta t}\frac{(r\,\Delta t)^n}{n!} \tag{2.17}$$

$$\langle n \rangle = r\,\Delta t \tag{2.18}$$

TODO: find a citation for this

where Δt denotes the integration time step of the simulator, which will be assumed to be $0.1ms$ from here on out. $\langle n \rangle$ denotes the expected number of spikes to be emitted in a simulation step, i.e. between $[t, t + \Delta t]$. Note that this mechanism makes the assumption that more than one spike can occur per simulation step. NEST was developed with this possibility in mind and provides a *multiplicity* parameter for Spike Events, which is processed at the postsynaptic neuron. As the high spike frequencies resulting from this could not occur in biological neurons, the model is also capable of simulating a refractory period. For this, the number of spikes per step is limited to 1, and the spiking probability is set to 0 for the duration of the refractory period t_{ref}. The probability of at least one spike occuring within the next simulation step is given the inverse probability of no spike occuring. Thus, when inserting $n = 0$ into Equation 2.17, the probability of eliciting at least one spike within the next simualtion step can be derived as:

$$P\{n \geq 1\} = 1 - e^{-r\Delta t} \tag{2.19}$$

---

compute nodes by the Simulator. A Multitude of Event types are provided (i.e. `SpikeEvent, CurrentEvent, RateEvent`), each able to carry specific types of payload and being processed differently by postsynaptic neurons.

Drawing from this probability then determines whether or not a spike is sent during that step, henceforth denoted with the function $s(t)$, which outputs 1 if a spike is sent during the interval $[t, t + \Delta t]$ **TODO: Notation correct?**, and 0 otherwise.

In order to implement the plasticity rule for spiking neurons, dendritic compartments need to be modeled with leaky dynamics. These dynamics are fundamentally the same as those described for the somatic compartment. Thus, the dendritic compartment of neuron j evolves according to:

$$C_m^{bas} \dot{v}_j^{bas} = -g_l^{bas} \, v_j^{bas} + \sum_{i \in I} W_{ji} s_i(t) \tag{2.20}$$

with presynaptic neurons I, and membrane capacitance C_m^{bas} and leakage conductance g_l^{bas} being specific to the basal dendrite. Note that these equations are calculated individually for each neuron and do not employ the matrix notation used for layers of rate neurons. Pyramidal apical and interneuron dendritic compartments evolve by the same principle and with largely the same parameters.

2.7   Event-based Urbanczik-Senn plasticity

One major challenge in implementing this architecture with spiking neurons is the Urbanczik-Senn plasticity introduced in Section 2.2. Since the plasticity rule is originally defined for rate neurons, computing the updates for spiking neurons requires some additional effort. Fortunately, this problem has already been solved in NEST for two-compartment neurons (Stapmanns et al., 2021). This Section will discuss its algorithm and implementation.

Since NEST is an event-based simulator, most of the plasticity mechanisms developed for it compute weight changes at the location (i.e. thread and compute node) of the postsynaptic neuron whenever an Event is received. This has several advantages; It allows the thread that created the Event to continue processing neuron updates instead of having to synchronize with all threads that manage recipient neurons. More importantly, this feature mirrors the local properties of biologically synaptic plasticity models, as these are often considered to be dependent on factors that are local to the synapse **TODO: cite**. For a spiking implementation of the Urbanczik-Senn plasticity, dendritic errors at every time step are required instead of just a scalar trace at the time of a spike, as would be the case for STDP. Thus, a mechanism for storing and reading these errors was requred, for which two basic possibilities were considered:

In a **Time-driven scheme**, dendritic errors are made available to synapses at every timestep, and weight changes are applied instantaneously. This approach requires very little memory, as no history of dendritic errors needs to be stored. It does come at the cost of

computational efficiency, since calls to the synaptic update function are as frequent as neuron updates - for all synapses. Particularly for large numbers of incoming synapses, as is common for simulations of cortical pyramidal neurons (Potjans and Diesmann, 2014; Vezoli et al., 2004), this implies a large number of function calls per time step. It also means that weight changes need to be computed at time steps where they are not immediately required (i.e. when there is no presynaptic activity), or when no weight change is necessary. Therefore, this approach proved costly in terms of Computational resources.

An **Event-driven scheme** on the other hand, updates synaptic weights only when a spike is sent through the synapse. A history of the dendritic error is stored at the postsynaptic neuron, which is read by each synapse when a spike is transmitted in order to compute weight changes. As the history of dendritic error applies equally to all incoming synapses, it only needs to be recorded once at the neuron. Alongside each entry in the history, a counter is stored and incremented whenever a synapse has read the history at that time step. Once all synapses have read out an entry, it is deleted. Thus, the history dynamically grows and shrinks during simulation and is only ever as long as the largest inter-spike interval (ISI) of all presynaptic neurons. This approach proves to be more efficient in terms of computation time, since fewer calls to the update function are required per synapse. It does come at the cost of memory requirements, as the history can grow particularly large for simulations with low in-degrees or large ISI[5]. During testing, the Event-based schemed proved substantially more efficient for many network types. This did however introduce the challenge of retroactively computing weight changes from the time of the last spike upon arrival of a new spike.

2.7.1 Integrating weight changes

Stapmanns et al. describe the Urbanczik-Senn plasticity rule based on the general form for weight changes

$$\dot{w}_{ij}(t) = F(s_j^*(t), V_i^*(t)) \tag{2.21}$$

where the change in weight $\dot{w}_{ij}$ of a synapse from neuron j to neuron i at time t is given by a function F that depends on the dendritic error of the postsynaptic neuron V_i^* and the presynaptic spiketrain s_j^*. The $*$ operator denotes a causal function, indicating that a value $V_i^*(t)$ potentially depends on all previous values of $V_i(t' < t)$. One can formally integrate

---

[5]It should also be noted that in this approach requires redundant integration of the history by every synapse. Stapmanns et al. propose a third solution, in which this integration is performed once whenever a spike is received, with the resulting weight change being applied to all synapses immediately. This approach proved to be even more efficient for some network configurations, but is incompatible with simulations where incoming synapses have heterogeneous synaptic delays due to the way that these delays are processed by the NEST simulator. See Section 3.1.3 in Stapmanns et al. (2021) for a detailed explanation.

Equation 2.21 in order to obtain the weight change between two arbitrary time points t and T:

$$\Delta w_{ij}(t,T) = \int_t^T dt' F[s_j^*, V_i^*](t') \tag{2.22}$$

This integral is of forms the basis of computing the change in weight between two arriving spikes. Thus, at the implementational level, t is usually the time of the last spike that traversed the synapse, and T is the current `biological_time`[6]. For spiking neurons, it is necessary to approximate the presynaptic activation ($\phi(u_j)$). For this, a well established solution is to transform the spiketrain s_j into a decaying trace using an exponential filter kernel κ:

$$\kappa(t) = H(t)\frac{1}{t}e^{\frac{-t}{\tau_\kappa}} \tag{2.23}$$

$$H(t) = \begin{cases} 1 & \text{if } t > 0 \\ 0 & \text{if } t \leq 0 \end{cases} \tag{2.24}$$

$$(f * g)(t) = \int_{-\infty}^{\infty} f(t')g(t-t')dt' \tag{2.25}$$

$$s_j^* = \kappa_s * s_j. \tag{2.26}$$

with filter time constant τ_κ. To obtain the trace of a spiketrain, it is convolved (Equation 2.25) with the exponential filter kernel κ. The filter uses the Heaviside step function $H(t)$, and is therefore only supported on positive values of t (also called a one-sided exponential decay kernel). This property is important, as integration limits of the convolution can be truncated when f and g are both only supported on $[0, \infty)$:

$$(f * g)(t) = \int_0^t f(t')g(t-t')dt' \tag{2.27}$$

Since spikes naturally only occur at $t > 0$, this simplified integral allows for a much more efficient computation of the spike train. In this particular case, the Function F on the right hand side of Equation 2.21 is defined as:

---

[6]This term is adopted from the NEST convention, where it describes the time for which a neuron or network has been simulated in *ms*. It describes how many simulation steps of length Δt *ms* have been computed, and is therefore independent from a simulation's runtime on the employed hardware (also called *wall clock time* (Van Albada et al., 2018)).

$$F[s_j^*, V_i^*] = \eta \kappa * (V_i^* s_j^*) \tag{2.28}$$

$$V_i^* = (\phi(u_i^{som}) - \phi(\hat{v}_i^{dend})) \tag{2.29}$$

this notation seems slightly abusive but is taken precisely from **Stapmanns et al.** **(2021)** with learning rate η. V_i^* then is the dendritic error of the dendrite that the synapse between j and i is located at[7]. Writing out the convolutions in Equation 2.22 explicitly, we obtain

$$\Delta w_{ij}(t, T) = \int_t^T dt' F[s_j^*, V_i^*](t') \tag{2.30}$$

$$= \int_t^T dt' \, \eta \int_0^{t'} dt'' \, \kappa(t' - t'') V_i^*(t'') s_j^*(t'') \tag{2.31}$$

Computing this Equation directly is computationally inefficient due to the nested integrals. Yet, it is possible to break up the integrals into two simpler computations and rewrite the weight change as:

$$\Delta W_{ij}(t, T) = \eta \left[I_1(t, T) - I_2(t, T) + I_2(0, t) \left(1 - e^{-\frac{T-t}{\tau_\kappa}} \right) \right] \tag{2.32}$$

$$I_1(a, b) = \int_a^b dt \, V_i^*(t) s_j^*(t) \tag{2.33}$$

$$I_2(a, b) = \int_a^b dt \, e^{-\frac{b-t}{\tau_\kappa}} V_i^*(t) s_j^*(t) \tag{2.34}$$

$$\tag{2.35}$$

See Section **TODO: ref** for a rigorous proof of this equation. The resulting equations allow for a rather efficient computation of weight changes compared to the complex integral described in Equation 2.31. This integration is performed whenever a spike traverses a synapse. It generalizes to all special cases in Equations 2.13-2.16, as long as the appropriate dendritic error is stored by the postsynaptic neuron.

---

[7]The dendritic error here is defined as the difference between two hypothetical rates based on the arbitrary function ϕ. The original implementation uses the difference between the actual postsynaptic spiketrain and this dendritic prediction ($V_i^* = (s_i - \phi(\hat{v}_i^{dend}))$). Furthermore, Stapmanns et al. show that generating a spiketrain from the dendritic potential ($V_i^* = (s_i - s_i^{dend})$) also results in successful learning, although at the cost of additional training time. This variant was chosen in order to not decrease learning performance any more than necessary.

2.8 Latent Equilibrium

The most significant drawback of the Sacramento model is the previously mentioned require-
ment for long stimulus presentation times and appropriately low learning rates. This makes
the network prohibitively inefficient for the large networks required for complex learning tasks.
Sacramento et al. developed a steady-state approximation of their network which does not
model the full neuron dynamics. It does not suffer from these issues and shows that their
model can in principle solve more demanding learning tasks such as MNIST. Yet these types
of approximation are much further detached from biological neurons than the original model
and thus do not lend themselves well to an investigation of biological plausibility (Gerstner
and Naud, 2009). Furthermore, they are incompatible with spike-based communication be-
tween neurons, since they require signal transmission between all connected neurons at every
simulation step, and do not model leaky membrane dynamics. Thus, neither the fully modeled
neuron dynamics nor the steady-state approximation are suited for complex learning tasks. A
substantial improvement to the model that promises to solve this dilemma was developed by
Haider et al. (2021), and will be discussed here.

When not relying on a steady-state approximation of neuron dynamics, the Sacramento
network is held back by the slow development of leaky neuron dynamics. When a stimulus-
target pair is presented to the network, somatic potentials in all neurons slowly increase until
a steady state is reached. The time until a network of leaky neurons has reached this state is
called the *relaxation period* following Haider et al. (2021). Given a membrane time constant
τ_m, a feedforward network with N layers of leaky neurons thus has a relaxation time constant
of $N\tau_m$. Yet in our case, a target activation simultaneously injected into the output neurons
slowly propagates backwards through the network. neurons at early layers require subsequent
layers to be fully relaxed in order to correctly compute their apical error terms, effectively
being dependent on two network passes. Haider et al. state that this kind of network therefore
requires $2N\tau_m$ before correct error terms are computed for a given input-output pairing.

This is a major issue, as it implies that plasticity during the first few miliseconds of a
stimulus presentation is driven by faulty error terms. The network thus tends to 'overshoot',
and needs to undo the synaptic weight changes made during the relaxation period in the later
phase of a stimulus presentation, in order to make tangible progress on the learning task.
Haider et al. call this issue the "relaxation problem" and suggest that it might be inherent to
most established attempts at biologically plausible Backpropagation algorithms (Whittington
and Bogacz, 2017; Guerguiev et al., 2017; Sacramento et al., 2018; Millidge et al., 2020).

The approach of increasing presentation time therefore is somewhat problematic. It im-
plicitly tolerates adverse synaptic changes at all levels of the network. Physiological changes
that are meant to immediately be undone are of course an inefficient use of a brain's resources,
which is highly undesirable for a biological system. More importantly, this kind of slow net-

work dynamics is likely too slow for the quick responses required for perception and aciton in the real world (Bartunov et al., 2018). One intuitive approach is to decrease synaptic time constants and remove the temporal filtering of stimulus injections. Yet this does not solve the fundamental issue, that a substantial portion of a stimulus presentation is defined by erroneous errors. Removing temporal filtering does decrease the relaxation period, but causes a drastic increase in dendritic errors during that period, effectively impeding learning. A possible approach to alleviate this issue is to disable plasticity for the first few milliseconds of stimulus presentation. After the network has relaxed the plasticity rules produce useful weight changes and learning rates can subsequently be increased. Yet a mechanism by which neurons could implement this style of phased plasticity is yet to be found, making this approach questionable in terms of biological plausibility. Ideally, the relaxation period would be skipped or shortened, in order to reduce erroneous plasticity. This would allow for a loosening of the constraints put on presentation time and learning rates, thus increasing computational efficiency.

The approach proposed by Haider et al. is to change the parameter of the activation function ϕ, a mechanism called *Latent Equilibrium*. Neurons in the original implementation (henceforth called *Sacramento neurons*) transmit a function of their somatic potential u_i, which is updated through euler integration at every simulation step (Equation 2.36). In contrast, neurons using Latent Equilibrium (henceforth called *LE neurons*) transmit a function of what the somatic potential is expected to be in the future. To calculate this expected future somatic potential $\breve{u}$, the integration is performed with a larger euler step:

$$u_i(t + \Delta t) = u_i(t) + \dot{u}_i(t) \ \Delta t \tag{2.36}$$

$$\breve{u}_i(t + \Delta t) = u_i(t) + \dot{u}_i(t) \ \tau_{eff} \tag{2.37}$$

Instead of broadcasting their rate based on the current somatic potential ($r_i(t) = \phi(u_i(t))$), LE neurons send their predicted future activation, denoted as $\breve{r}_i(t) = \phi(\breve{u}_i(t))$. The degree to wich LE neurons look ahead is determined by the *effective membrane time constant* $\tau_{eff} = \frac{C_m}{g_l + g^{bas} + g^{api}}$. This time constant takes into account the conductance with which dendritic compartments leak into the soma, which is a key driving factor for the speed at which the network relaxes. Any computations that employ or relate to this prediction of future network states will henceforth be referred to as *prospective* and denoted with $\breve{\ }$.

When employing the default parametrization given by Haider et al. **TODO: reference parameter table**, τ_{eff} is slightly lower than reported pyramidal neuron time constants (McCormick et al., 1985) at approximately $5.26ms$. While employing prospective dynamics does not alter activations and weights at the input layer, neurons at subsequent layers approach their steady state much more quickly, as depicted in Figure 2.2. This property extends to the local error terms of pyramidal- and interneurons, which relax much faster for LE networks, as
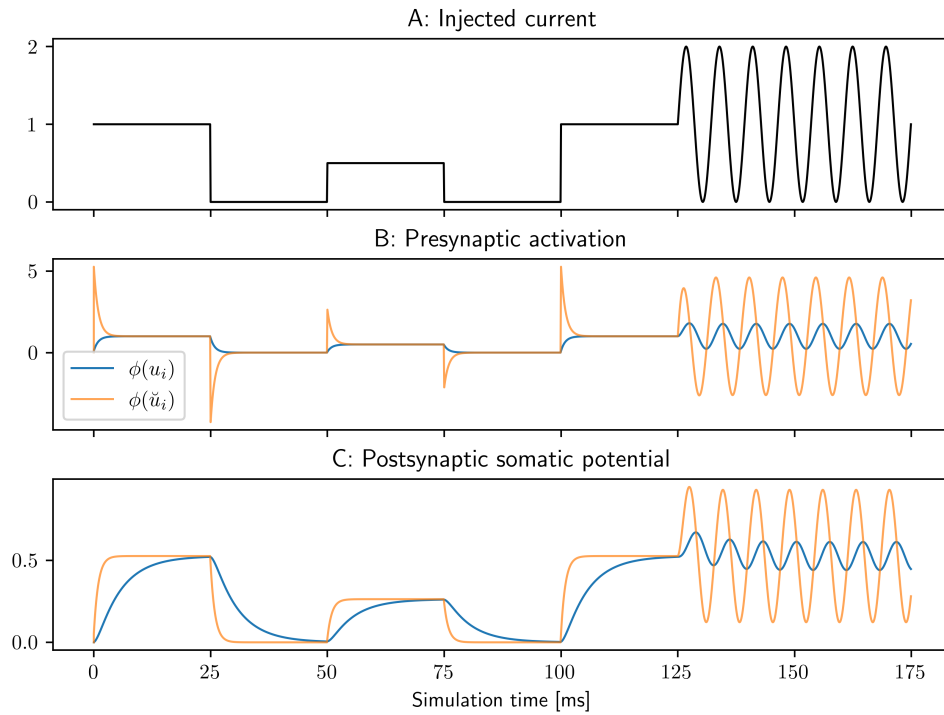
Figure 2.2: Signal transmission between an input neuron i and a hidden layer pyramidal neuron j. Depicted are activations for the original Sacramento model and prospective activation using Latent Equilibrium. **A:** Current injected into both types of neurons. **B:** Activation of the input neuron using Sacramento dynamics $\phi(u_i)$ (blue), and prospective activation $\phi(\breve{u}_i)$ (orange). Note how strongly prospective activation reacts to changes in somatic voltage, leading to jumps in activation. After the input neuron has reached its relaxed state ($\dot{u}_i = 0$), both types of neuron evoke the same activation. **C:** Somatic potential u_j of the pyramidal neuron responding to signals sent from the input neuron (color scheme as in B).

shown in Figure 2.3. In the idealized case considered in the original paper, the signal transmission in a feedforward network is immediate, despite membrane potentials not necessarily catching up. These results highlight the superiority of LE for learning in this network, as network relaxation is almost instantaneous. In contrast, the error terms in a Sacramento network drive random synaptic plasticity even when the network is fully trained on a given dataset and is able to make accurate predictions. Thus, both the issue of redundant weight changes, as well as the concern over response and learning speed can be solved by LE.

In addition to using the prospective somatic potential for the neuronal transfer function, it is also used in the plasticity rule of LE neurons. The Urbanczik-Senn plasticity is therefore updated to compute dendritic error from prospective somatic activations and a non-prospective dendritic potential $\dot{w}_{ij} = \eta \ (\phi(\breve{u}_i^{som}) - \phi(\hat{v}_i^{bas})) \ \phi(\breve{u}_j^{som})^T$. Much like for the transfer function, this change serves to increase the responsiveness of the network to input changes.

TODO: keep the following section? Besides the using a prediction of future somatic
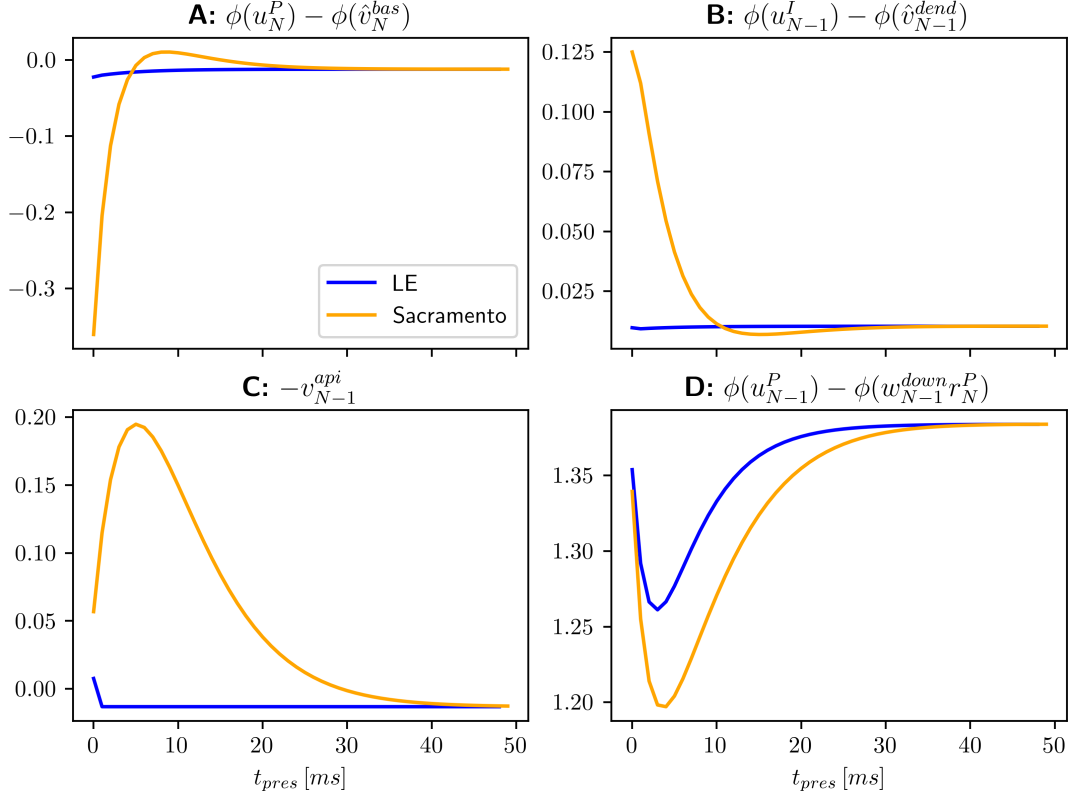
Figure 2.3: Effects of Latent equilibrium on relaxation of the dendritic error terms from Equations 2.13-2.16. Depicted are error terms for individual neurons of a network with one hidden layer that was fully trained on the Bars dataset **TODO: ref**. When employing Sacramento dynamics (orange), dendritic errors exhibit longer and more intense deviations, while errors in an identical LE network (blue) relax much sooner. Note, that errors do not decay exactly to zero due to the fluctuations inherent to the spiking network variant. **A:** Basal dendritic error for a pyramidal neuron at the output layer. **B:** Dendritic error for a hidden layer Interneuron. **C:** Proximal apical error for a hidden layer Pyramidal neuron. For this case the difference between the two networks is most striking, as errors for the LE network exhibit almost no deviation from rest. **D:** Distal apical error for the same pyramidal neuron. Note that this error term does not converge to zero for either network even after training is complete, which will be discussed in Section 5.4.

activity for neuronal transfer and plasticity, Haider et al. (2021) further alter the plasticity rule by means of their implementation. While the simulations by Sacramento et al. (2018) strictly conforms to the equations above, the new implementation (GitHub) . The fundamental building block of a network here is a layer, which is represented in code as an instance of the class `Layer`. Each instances holds information about its corresponding pyramidal- and interneurons. It also holds information about the synaptic connections between the two populations, as well as all incoming feedforward and feedback pyramidal synapses. A layer has two class methods that are fundamental to its computation; `update()` computes membrane potential derivatives and synaptic weight changes given pyramidal neuron activations from the previous and subsequent layers. `apply()` updates weights and membrane potentials from the previously calculated changes. Layers are processed in order from input to output layer,

where all of them receive the `update()` signal first, before `apply()` is called on all of them. This ordering ensures, that changes in activation do not cascade through the layers and lead to excessive activations at the output. Yet, since next layer activations at time t have not been computed, top down information is always delayed by one timestep. **TODO: evaluate importance of this**

Thus, the equations for membrane updates change slightly:

2.9 Implementational details

Building on the neuron and plasticity model from Stapmanns et al. (2021), a replicate model of the pyramidal neuron with spiking communication was developed in NEST. The existing Urbanczik-Senn neuron was expanded to three compartments, and storage and readout of dendritic errors were updated to allow for compartment-specific plasticity rules. Interneurons were chosen to be modeled as pyramidal neurons with slightly updated parameters and apical conductance $g^{api} = 0$. Since membrane dynamics of both neurons follow the same principles and additional compartments have minor impact on performance, this was deemed sufficient.

After facing some setbacks when attempting to train the first spiking variant of the network, the decision was made to also implement a rate-based variant of the neuron in NEST. While the additional effort required for another implementation might be questionable, this model turned out to be indispensable. It enabled the identification of both errors in the model, as well as training mechanisms and parameters that required changes to enable spike-compatible learning.

Following NEST convention, the spiking and rate-based neuron models were named `pp_cond_exp_mc_pyr`[8] and `rate_neuron_pyr` respectively. Furthermore, the `pyr_synapse` class was defined for spike events, and implements a variant of the event-based Urbanczik-Senn plasticity described in Section 2.7. The `pyr_synapse_rate` model on the other hand transmits rate events and updates its weight according to the original plasticity rule.

Simulations were managed using the python API `PyNEST` (Eppler et al., 2009), which is much more convenient than the SLI interface that lies at the core of NEST. An additional advantage of using this language is, that the LE network from (Haider et al., 2021) is also implemented in python. Thus, by including a slightly modified version of that code in my project, it was possible to unify all three variants in a single network class and accompanying interface. This allowed for exact alignment of network stimulation and readout and enabled in-depth comparative analyses. In the upcoming Result, three variants of the same network architecture will therefore be compared; The modified python implementation from (Haider et al., 2021) is termed `NumPy` based on the framework that is used to compute neuron dynamics and synaptic plasticity through matrix multiplication. The two NEST variants will be referred

---

[8]Despite being somewhat cryptic, the name does actually make sense, as it describes some key features of the model: It is a **point process** for **cond**uctance based synapses and has an **exp**onentially decaying membrane in **multiple compartments**.

to as *NEST spiking* and *NEST rate.* The NEST rate version will serve to distinguish differences that are due to the novel simulation backend from those that were introduced by the spike-based communication scheme.

2.9.1   Neuron model Adaptations

The neuron model from Stapmanns et al. (2021) was modified in some ways in order to remove unnecessary parameters and match the pyramidal neuron implementation more closely. Both the inclusion of nonzero reversal potentials and the flow of currents from the soma to the dendrites were omitted in my model. **TODO: argue?** Furthermore, the present network requires synapses to be able change the sign of their weight at runtime, which is not permitted in the original synapse model. For this reason, the strict separation of excitatory and inhibitory synapses had to be removed from the synapse model. In order to compare the different implementations exactly, the ODE solver with variable stepsize was replaced with Euler integrations[9] with step size Δt. For the spiking neuron model, dendritic compartments are modeled with leaky membrane dynamics in contrast to the rate variant. The choice of dendritic leakage conductance $g_l^{dend} = \Delta t$ is motivated in Section 5.3.

A major issue of the spiking network is the fact that under the default parametrization, spikes are too infrequent for the network to relax quickly and accurately encode dendritic errors. Initial experiments showed that the network is sensitive to changes in parametrization, which meant that it was desirable to change as few existing parameters as possible. Therefore, a novel parameter ψ was introduced. In a spiking neuron i, the probability of eliciting a spike is linearly increased by this factor ($r_i = \psi\phi(u_i)$). Likewise, all synaptic weights W in a spiking network are attenuated by the same factor ($W \leftarrow \frac{W}{\psi}$). These changes cancel each other out, as a change in ψ elicits no change in absolute compartment voltages of a network. Instead, it serves to stabilize these voltages over time, which drastically improves learning performance of the network. One mechanism in which this parameter needs to be considered is the plasticity rule. Weight changes are affected by ψ in three distinct ways: The dendritic error scales linearly with ψ, as does the presynaptic activation. Additionally, since the frequency of weight changes is determined by the presynaptic spike rate, learning rates are attenuated by $\eta \leftarrow \frac{\eta}{\psi^3}$. The exception to this are the weights from interneurons to pyramidal neurons, as these do not depend on dendritic predictions, but on absolute dendritic voltage. Hence, in this case $\eta^{pi} \leftarrow \frac{\eta^{pi}}{\psi^2}$. On close investigation of the spiking neuron model, one can observe that for $\psi \rightarrow \inf$, it becomes an exact replication of the rate-based implementation. Unsurprisingly therefore, increasing ψ caused the spiking network to learn successfully with fewer samples and to a lower test loss. The argument against increasing ψ is twofold: Initial experiments showed that with $\psi \in [0.5, 1]$, pyramidal and interneurons exhibit spike frequencies in biologically plausible range of less than $55Hz$ Kawaguchi (2001); Eyal et al. (2018). Additionally, each

---

[9]This change initially served debugging purposes, but turned out to have no negative effect on efficiency and was therefore kept

transmitted `SpikeEvent` is computationally costly, which increases training time (cf. Figure 3.6) and further makes high spike frequencies undesirable. As a middle ground, $\psi = 100$ proved useful during initial tests and will be assumed the default from here on out.

With these adaptations, the network was able to perform supervised learning with spiking neurons, as will be discussed in the upcoming sections.

Chapter 3

Results

TODO: Today, I changed the test criterion from the output neuron voltage at time t to a mean over a sample of the last $20ms$, network performance improved tremendously. Intuitively makes sense, but in particular it makes NEST networks diverge less after peak performance is reached. Are fluctuations in output layer activity increasing during late stages of training?

TODO: it might be worth experimenting with different synaptic delays in NEST in order to evaluate learning performance under biologically plausible transmission times. How easy this will assumably be to implement in NEST deserves note at this point.

TODO: talk about the fact that NEST synapses are updated, and SpikeEvents stored to ring buffers to be integrated into u_som after the synaptic delay. How much of physiological synaptic delays occurs pre- and postsynaptically in pyramidal neurons?

3.1   direct feedback connections to interneurons

Vaughn and Haas (2022); Mancilla et al. (2007)

3.2   The self-predicting state

As a first comparison between the three implmementations, the pre-training towards a self-predicting stat (cf. Sacramento et al. (2018) Figure S1) was performed with equal parametrizations, as shown in Figure 3.1. For this experiment, no target signal was provided at the output layer, and the network was stimulated with random inputs.

All implementations were able to reach comparable values for the four error metrics after roughly the same time. The exact values that errors converge on differs slightly between implementations, but generally is on the same order of magnitude and thus does not hinder
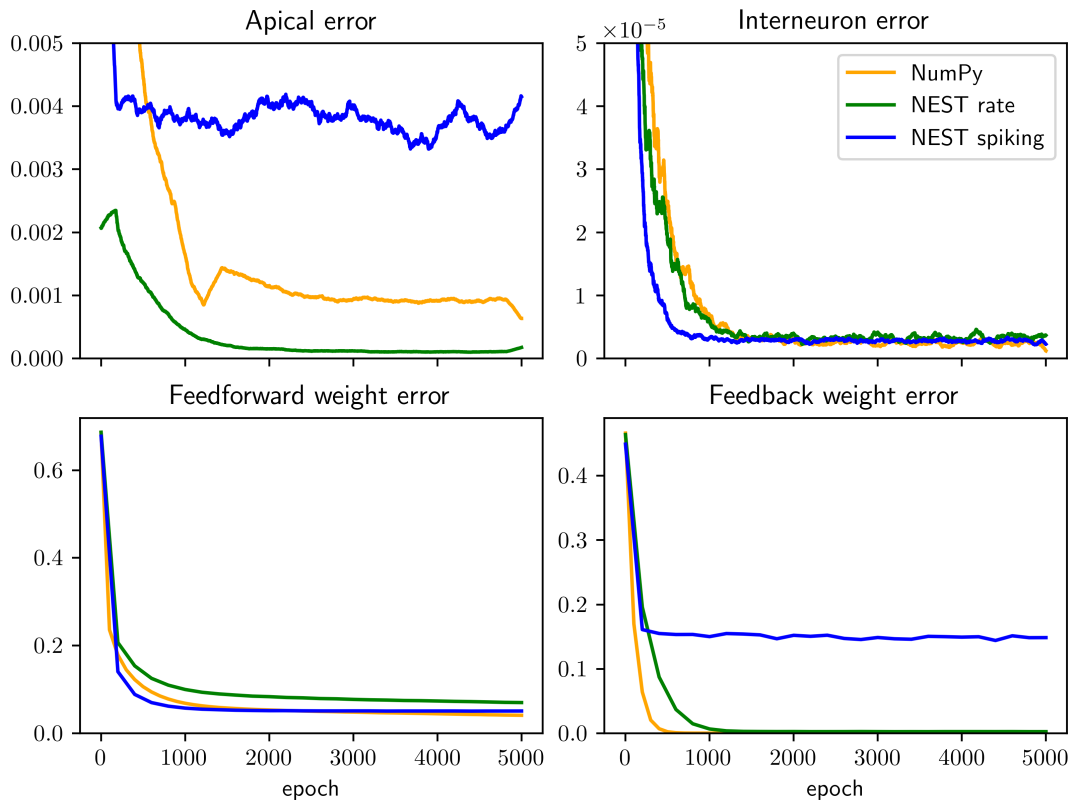
28

Figure 3.1: Different network types learn to predict self-generated activity in superficial layers. All networks were initialized with dimensions $[6, 10, 3]$, and stimulated with 5000 samples of random input for $100ms$ each. As described in Sacramento et al. (2018), during only Pyramidal-Interneuron and Interneuron-Pyramidal weights are plastic ($\eta^{pi} = 0.05, \eta^{ip} = 0.02375, \eta^{up} = \eta^{down} = 0$). All variants reach a self-predicting state within the first 1000 stimulus presentations and errors remain stable after that point.

learning performance greatly (cf. Section 3.3). A notable outlier is the apical error of pyramidal neuron in the spike-based implementation. This can however be traced back to individual spikes causing substantial deviations in apical potentials, and can therefore be alleviated by increasing the *weight_scale* parameter (results not shown) at the cost of increased training time. Alternatively, increasing the membrane capacitance of the apical compartment also solves the issue as it smoothes out the effect of individual spikes. Yet this solution also increases the relaxation period of the entire network, requiring a highly undesirable increase in t_{pres} for successful learning. Since weight errors converge to similar values as the rate-based implementations, an increased absolute apical compartment voltage was deemed tolerable.

3.3 Presentation times with latent equilibrium

In order to validate the performance of my implementations, I replicated a parameter study from Haider et al. (2021)[Fig. 3]. The results for the NEST network using spiking neurons with default parameters **TODO: elaborate on this** are shown in Figure 3.2. A
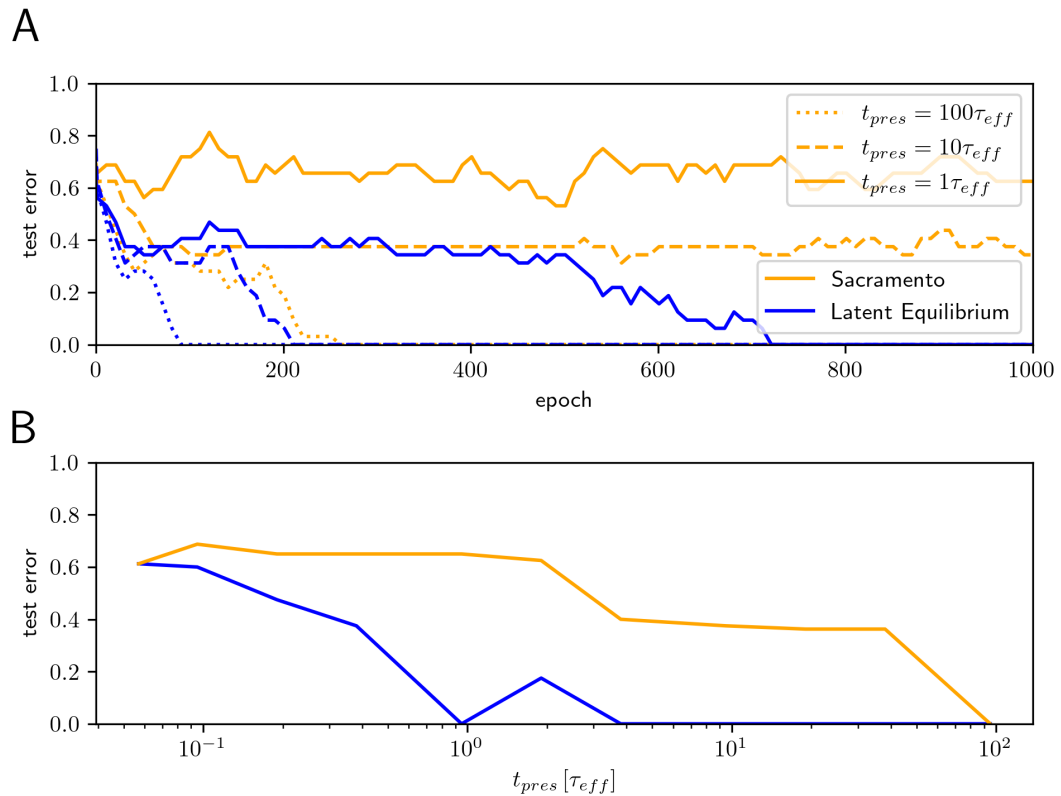
Figure 3.2: Replication of Figure 3 from Haider et al. (2021) using networks of spiking neurons in the NEST simulator. **A:** Comparison between Original pyramidal microcircuit network by Sacramento et al. (2018) and Latent equilibrium variant from Haider et al. (2021). Shown is the training of a network with 9-30-3 neurons on the 'Bars' Dataset from **TODO: describe it** with three different stimulus presentation times. **B:** Test performance after 1000 Epochs as a function of stimulus presentation time.

3.4 Separation of synaptic polarity

A key limitation of the present network model is the requirement that all synapses must be able to assume both positive and negative polarities. When restricting any synaptic population in the network to just one polarity, the network is unable to reach the self-predicting state **TODO: expand?**. Thus, activity in any neuron must be able to have both excitatory and inhibitory postsynaptic effects facilitated by appropriate synaptic weights. This requirement is at odds with biology, which dictates a singular synaptic polarity for all outgoing connections of a neuron, determined by neuron type and its corresponding neurotransmitter **TODO: cite**.

To investigate to what degree the plasticity rule can deal with this constraint, an experiment was conducted: A population of pyramidal neurons A was connected to another population C with plastic synapses that were constrained to positive weights. In order to facilitate the required depression, A was also connected to a population of inhibitory interneurons B through excitatory synapses with random and non-plastic weights. The interneurons in turn were connected to C through plastic, inhibitory connections. All incoming synapses at C targeted the same dendritic compartment. When inducing a dendritic error in that compartment, all
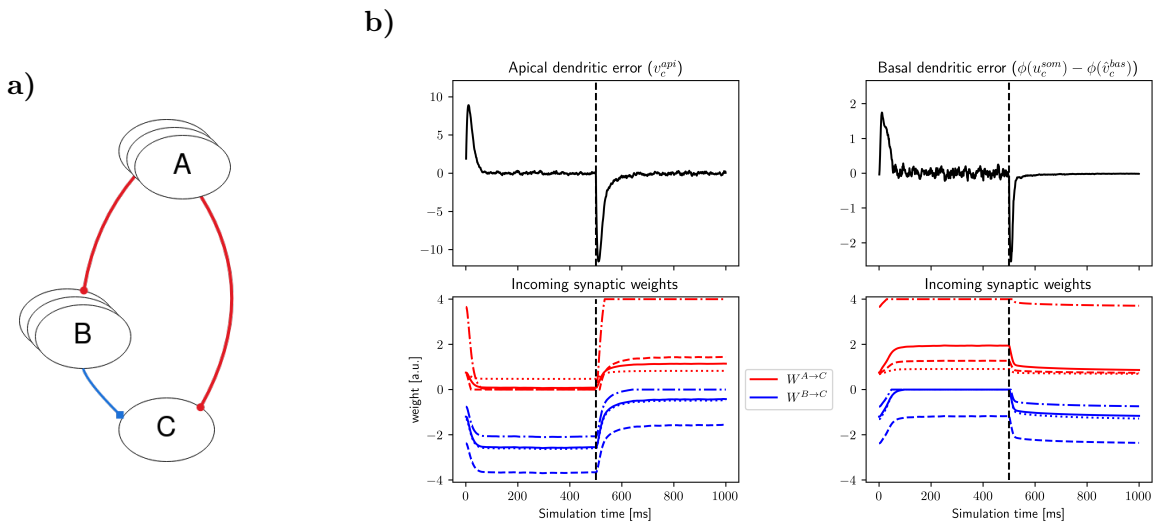
b)

a)

Figure 3.3: Dendritic error minimization under biological constraints on synaptic polarity and network connectivity. **a)** Network architecture. An excitatory population *A* connects to a dendrite of Neuron *C* both directly and through inhibitory interneuron population *B*. Only synapses $A \to C$ and $B \to C$ are plastic through dendritic error rules. Populations *A* and *B* are fully connected with random weights. **b)** *Left:* All plastic synapses arrive at apical dendrites and evolve according to Equation 2.15. *Right:* Identical network setup, plasticity for synapses at basal dendrites (Equations 2.13, 2.14). *Top:* Dendritic error of a single target neuron. Errors of opposite signs are induced at 0 and 500*ms* (vertical dashed line). *Bottom:* Synaptic weights of incoming connections. All initial synaptic weights and input neuron activations were drawn from uniform distributions.

plastic synapses in the network collaborated in order to minimize that error. When injecting a positive basal error for example, the inhibitory weights $(C \to B)$ decayed, while excitatory synaptic weights $(A \to B)$ increased. Flipping the sign of that error injection had the opposite effect on weights, and likewise cancelled the artificial error. This shows that a separation of synaptic polarity does not interfere with the principles of the Urbanczik-Senn plasticity when depression is facilitated by interneurons.

Yet, as criticised previously (Whittington and Bogacz, 2019), the one-to-one connections between *A* and *B* are untypical for biological neural networks **TODO: cite**. Hence, a second experiment was performed, in which *A* and *B* were fully connected through static synapses with random positive weights. This decrease in specificity of the connections did not hinder the error-correcting learning, as shown in Figure 3.3.

These results are useful, as they enable a biologically plausible way for excitatory long-range pyramidal projections to connect to pyramidal neurons in another layer (i.e. in a different part of the cortex). The steps required to facilitate this type of network are rather simple; A pyramidal neuron projection could enter a distant cortical area and spread spread its axonal tree **phrasing**within a layer that contains both pyramidal neuron dendrites and interneurons. If these interneurons themselves connect to the local pyramidal population, Errors with arbitrary signs and magnitudes in those dendrites could be effectively minimized by the described connectivity. While error minimization is a funcamental feature of this network, it does not
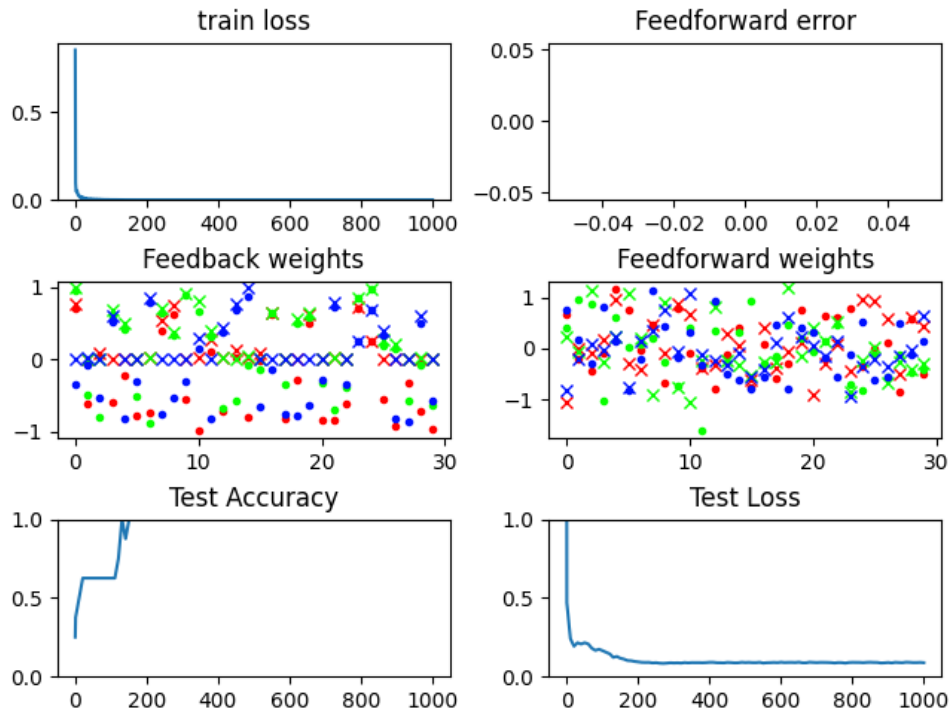
Figure 3.4: Training progress of a network of rate neurons in NEST, in which hidden layer connections between interneurons and pyramidal neurons are unipolar and nonspecific.

necessarily imply that synaptic credit assignment is successful aswell. To prove that this nonspecific connectivity does not hinder learning, it was introduced into the dendritic error network. The connection between Interneurons and Pyramidal neuron apical dendrites was chosen for the first test, as the employed plasticity rule had proven most resilient to parameter imperfections previously. A network of rate neurons was initialized with self-predicting weights as in Section 3.3. The Weights w^{pi} were redrawn and restricted to postive values, and a secondary inhibitory interneuron population was prepared and fully connected to both populations as described in Figure 3.3.

3.5 In search of plausible spike frequencies

TODO: expand

3.6 Resilience to imperfect connectivity

3.7 Performance of the different implementations

As stated in Haider et al. (2021), simulating the present network with many neurons or more than one hidden layer quickly becomes unfeasible when simulating the full leaky dynamics. To investigate how network size affects simulation time, all three implementations created for this
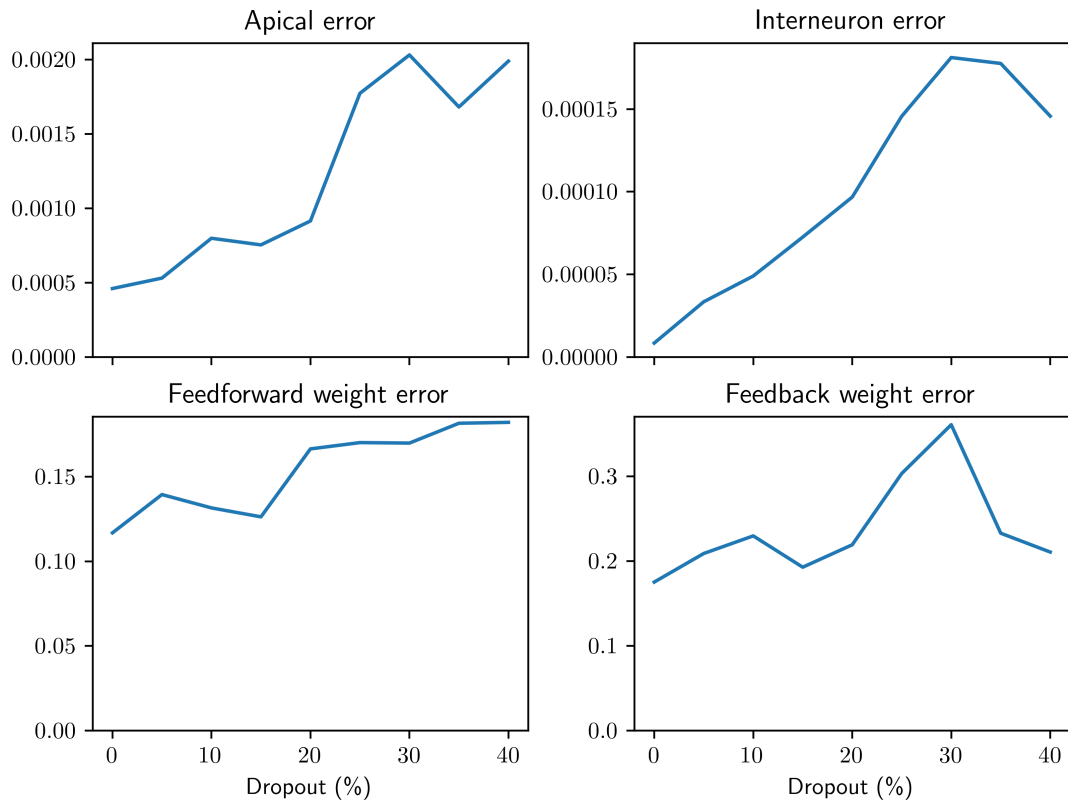
Figure 3.5: Error terms after training a network with dimensions [8, 8, 8] towards the self predicting states, with different percentages of synaptic connections randomly removed. To avoid completely separated layers, synapse deletion was performed per synaptic population, and the percentage is therefore only an approximation. Even with only 60% of synaptic connections present, the network architecture still achieves competetive values for all four error metrics. For the weight errors, which is calculated with mean-squared-error over two matrices, missing synapses were set to 0. This choice was made under the assumption that a missing connection in an ideal self-predicting network would be matched by a zero-weight - or likewise absent - synapse. Experiments were performed with the rate-based network in NEST, each network was trained fro 2000 epochs of 50ms each.

project were trained on the bars dataset for a single epoch with different network sizes for a single epoch, in order to assess efficiency.

The result of this comparison is shown in Figure 3.6. The NumPy network is slow at baseline, which is likely explained by the fact that it is the only variant which is running on a single thread. This is due to a limitation of NumPy, and could likely be improved greatly by using batched matrix multiplications, as are provided for example by `PyTorch`[1]. Notably, this variant exhibits very little slowdown in response to an increase in network size. My assumption is, that the vectorization of synaptic updates on a single thread scales up better than the communication between threads that is required by most events in the NEST

---

[1]It is also possible, that the network code surrounding the NumPy computations is less efficient than the one for the NEST network. As this implementation was needed primarily to prove that neuron dynamics and synaptic updates were ported correctly to NEST, efficiency was a minor concern here and this was not investigated further.
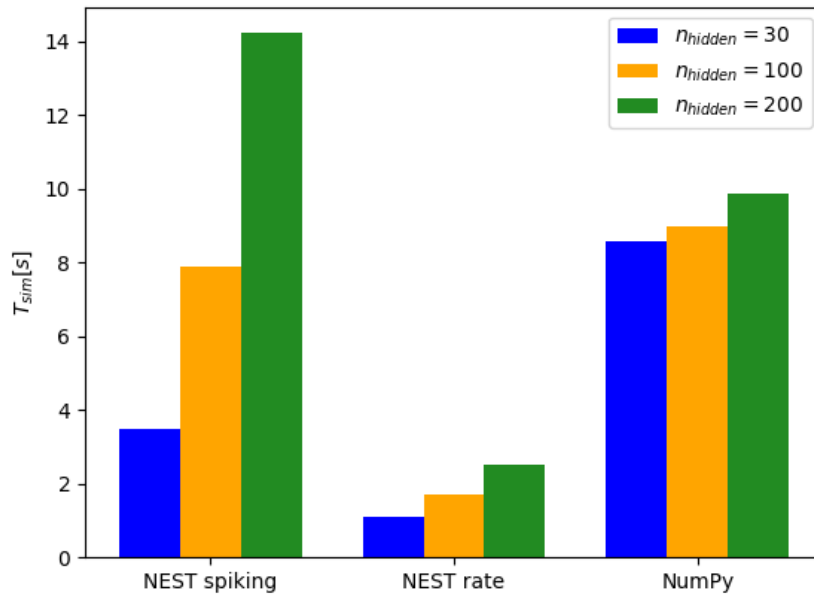
Figure 3.6: Benchmark of the three different implementations using a network of $[9, n_{hidden}, 3]$ neurons per layer. $n_{hidden} = 30$ was chosen as a baseline, as it is the default throughout all simulations on the Bars dataset. Networks were instantiated with the same synaptic weights and trained for a single epoch of 5 stimulus presentations of $100ms$ each. Simulations were performed on an *AMD Ryzen Threadripper 2990WX* using 8 cores for the NEST simulations at up to $3.0GHz$.

simulations. The NEST implementation using rate neurons performed best in terms of speed across the board. This result was slightly surprising, as the demand on the communication interface between threads is very high, since all neurons transmit an event to each of their postsynaptic targets at every time step.

Finally, the novel spiking variant of this model performed substantially worse than antici-pated. Particularly in comparison to the rate implementation, I initially expected substantial performance improvements. The Difference between the two was even greater when simulating on an office-grade processor (Benchmark was also run on an *Intel Core i5-9300H* at $2.40GHz$, results not shown). Three hints about the comparatively poor performance can be deduced: For one, both the rate and the spiking neuron model employ almost identical neuron models, with minor changes to parametrization and output generation. Thus, updates to the neuron state are unlikely to be responsible for the worse performance. Secondly, the number of Events transmitted between neurons is much lower for the SNN compared to

the *relative* performance decrease when increasing the number neurons by the same amout is much greater for the spiking network. Thus, the most likely cause of slowdown are the updates at the synapses. This is supported by the fact, that the number of synapses increases much faster for this kind of network than the number of neurons. For the given network of

$n_x = 9$ input neurons, $n_y = 3$ output neurons and n_h neurons in the hidden layer l, the number of total synapses in the network is given by

$$n_{synapses} = |w_l^{up}| + |w_l^{pi}| + |w_l^{ip}| + |w_l^{down}| + |w_y^{up}| \tag{3.1}$$

$$= n_h n_x + n_h n_y + n_y n_h + n_h n_y + n_y n_h \tag{3.2}$$

$$= n_h(n_x + n_y^4) \tag{3.3}$$

with $|w|$ of a weight matrix w in this case denoting the total number of elements in that matrix **Is there a more conventional notation?** . Thus, the number of synapses in a network grows much faster than the number of total neurons when increasing the size of the hidden layer.

availis given by the stark increase in

3.8   Response to unpredicted stimuli

The activity of many cortical neurons increases when a brain is presented with unpredicted stimuly that regard these neurons **TODO: check out** Whittington and Bogacz **(2019) refs 50-54**. This property is prominently replicated by predictive coding networks, since activation of error nodes is a function of local prediction errors. Prediction errors in the present model on the other hand are encoded in both positive and negative potentials of apical dendrites. Hence, the
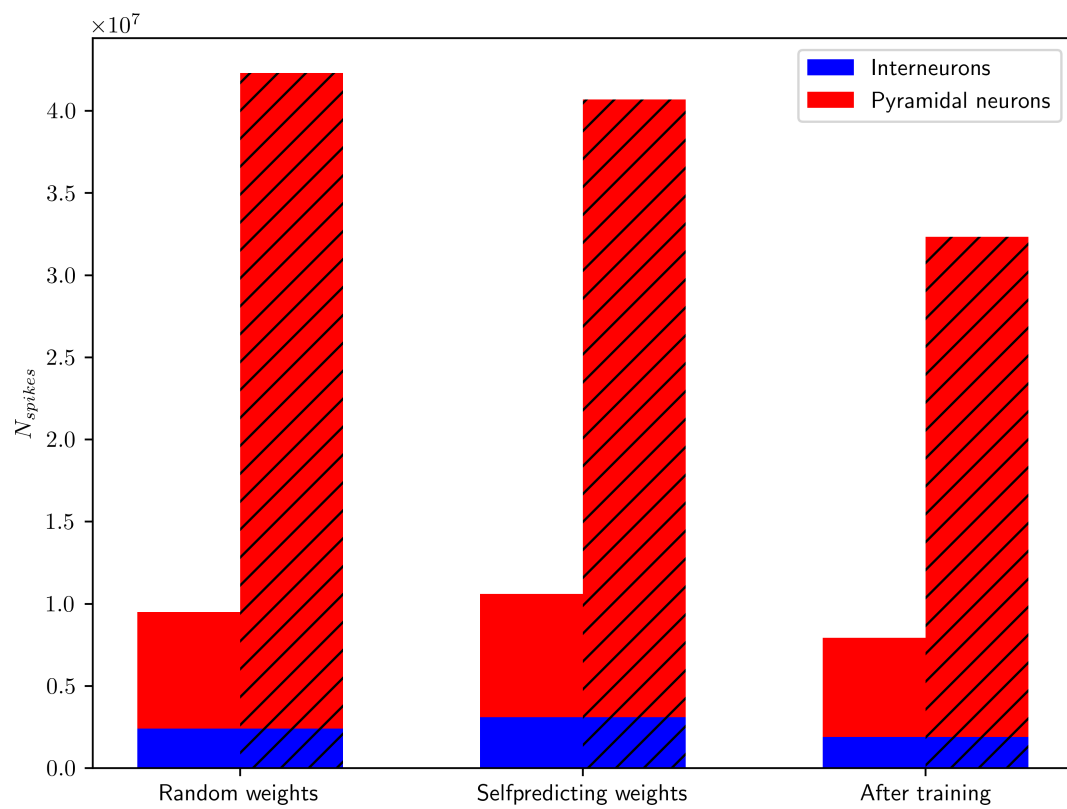
Figure 3.7: Comparison of network response to stimuli from the Bars dataset.

Chapter 4

Discussion

4.1 Limitations of the implementation

Network needs to be reset between stimuli original does not do that, in NEST it's kindof a big deal.

exposure time and training set still quite large

non-resetting, non-refractory

4.2 Whittington and Bogacz criteria

In which we discuss, to what extent the network conforms to the criteria for biologically plausible learning rules introduced by Whittington and Bogacz (2017):

1. Local computation. A neuron performs computation only on the basis of the inputs it receives from other neurons weighted by the strengths of its synaptic connections.

2. Local plasticity. The amount of synaptic weight modification is dependent on only the activity of the two neurons the synapse connects (and possibly a neuromodulator).

3. Minimal external control. The neurons perform the computation autonomously with as little external control routing information in different ways at different times as possible.

4. Plausible architecture. The connectivity patterns in the model should be consistent with basic constraints of connectivity in neocortex.

4.3 Should it be considered pre-training?

TODO: someone said this network needs pre-training and that made me sad :(

4.4 Relation to energy minimization

4.5 Correspondence of the final model to cortical circuitry

Cortical neurons depend on neuromodulation too Roelfsema and Holtmaat (2018)

Completely unclear whether cortical circuits perform supervised learning (Magee and Grienberger, 2020)

4.6 Outlook

This would probs be super efficient on neuromorphics!

I am not going to try plasticity with spike-spike or spike-rate dendritic errors

Training on ImageNet

Making this shit faster

BPTT

4.6.1 improvements to the neuron models

improve prospective activity with regard to spike creation

le does a lot, particularly at hidden layers. Yet response time under spiking paradigms is still lackluster. In particular, prospective activation does next to nothing for these very low input time constants. SNN performs best when τ_x is greater than Δ_t by roughly x10.

foo

TODO: talk about ALIF neurons (Gerstner and Naud, 2009) also reffed in e-prop(Bellec et al., 2019, 2020). look for sources

pyr and intn are wayy to similar

LIF, membrane reset and t_{ref}

reward-modulated urbanczik-senn plasticity?

wtf is shunting inhibition?

4.6.2 improvements to the network

think about recurrence?

Chapter 5

Appendix

5.1 Somato-dendritic coupling

Urbanczik and Senn (2014) discuss a possible extension to their neuron- and plasticity model, in which the dendro-somatic coupling transmits voltages in both directions. They show that the plasticity rule requires only minor adaptations for successful learning under this paradigm. Yet, as described by passive cable theory, the flow between neuronal compartments is dictated by their respective membrane capacitances. These are calculated from their membrane areas, which vastly differ in the case of pyramidal neurons. **TODO: find a nice citation for this**

15,006 458

will not be considered here. The motivation is, that dendritic membrane area is

5.2 Integration of the spike-based Urbanczik-Senn plasticity

Starting with the complete Integral from $t = 0$.

$$\dot{W}_{ij}(t) = \eta(\phi(u_i) - \phi(\alpha v_i^{basal}(t)))\phi(u_j) \tag{5.1}$$

$$\Delta W_{ij}(t,T) = \int_t^T dt' \ \eta \ (\phi(u_i^{t'}) - \phi(\widehat{v_i^{t'}})) \ \phi(u_j^{t'}) \tag{5.2}$$

$$\Delta W_{ij}(t,T) = \eta \int_t^T dt' \ (\phi(u_i^{t'}) - \phi(\widehat{v_i^{t'}})) \ \phi(u_j^{t'}) \tag{5.3}$$

$$V_i^* = \phi(u_i^{t'}) - \phi(\widehat{v_i^{t'}}) \tag{5.4}$$

$$s_j^* = \kappa_s * s_j \tag{5.5}$$

$$\Delta W_{ij}(0,t) = \eta \int_0^t dt' \ \int_0^{t'} dt'' \ \kappa(t' - t'')V_i^*(t'')s_j^*(t'') \tag{5.6}$$

$$= \eta \int_0^t dt'' \ \int_{t''}^t dt' \ \kappa(t' - t'')V_i^*(t'')s_j^*(t'') \tag{5.7}$$

$$= \eta \int_0^t dt'' \ \left[\tilde{\kappa}(t - t'') - \tilde{\kappa}(0) \right] V_i^*(t'')s_j^*(t'') \tag{5.8}$$

$$\tag{5.9}$$

With $\tilde{\kappa}$ being the antiderivative of κ:

$$\kappa(t) = \frac{\delta}{\delta t} \tilde{\kappa}(t) \tag{5.10}$$

$$\tilde{\kappa}(t) = -e^{-\frac{t}{\tau_\kappa}} \tag{5.11}$$

$$\tag{5.12}$$

The above can be split up into two separate integrals:
Which implies the identities

$$I_1(t_1, t_2 + \Delta t) = I_1(t_1, t_2) + I_1(t_2, t_2 + \Delta t) \tag{5.13}$$

$$I_2(t_1, t_2 + \Delta t) = e^{-\frac{t_2 - t_1}{\tau_\kappa}} I_2(t_1, t_2) + I_2(t_2, t_2 + \Delta t) \tag{5.14}$$

$$I_2(t_1, t_2 + \Delta t) = -\int_{t_1}^{t_2 + \Delta t} dt' \ \tilde{\kappa}(t_2 + \Delta t - t') V_i^*(t') s_j^*(t') \tag{5.15}$$

$$= -\int_{t_1}^{t_2} dt' \left[-e^{-\frac{t_2 + \Delta t - t'}{\tau_\kappa}} \right] V_i^*(t') s_j^*(t') - \int_{t_2}^{t_2 + \Delta t} dt' \left[-e^{-\frac{t_2 + \Delta t - t'}{\tau_\kappa}} \right] V_i^*(t') s_j^*(t') \tag{5.16}$$

$$= -e^{-\frac{\Delta t}{\tau_\kappa}} \int_{t_1}^{t_2} dt' \left[-e^{-\frac{t_2 - t'}{\tau_\kappa}} \right] V_i^*(t') s_j^*(t') - \int_{t_2}^{t_2 + \Delta t} dt' \left[-e^{-\frac{t_2 + \Delta t - t'}{\tau_\kappa}} \right] V_i^*(t') s_j^*(t') \tag{5.17}$$

Using this we can rewrite the weight change from t to T as:

$$\Delta W_{ij}(t, T) = \Delta W_{ij}(0, T) - \Delta W_{ij}(0, t) \tag{5.18}$$

$$= \eta [-I_2(0, T) + I_1(0, T) + I_2(0, t) - I_1(0, t)] \tag{5.19}$$

$$= \eta [I_1(t, T) - I_2(t, T) + I_2(0, t) \left(1 - e^{-\frac{T-t}{\tau_\kappa}} \right)] \tag{5.20}$$

The simplified Sacramento et al. (2018) case would be:

$$\frac{dW_{ij}}{dt} = \eta (\phi(u_i) - \phi(\hat{v}_i)) \phi(u_j) \tag{5.21}$$

$$\Delta W_{ij}(t, T) = \int_t^T dt' \ \eta \ (\phi(u_i^{t'}) - \phi(\widehat{v_i^{t'}})) \ \phi(u_j^{t'}) \tag{5.22}$$

$$\Delta W_{ij}(t, T) = \eta \int_t^T dt' \ (\phi(u_i^{t'}) - \phi(\widehat{v_i^{t'}})) \ \phi(u_j^{t'}) \tag{5.23}$$

$$V_i^* = \phi(u_i^{t'}) - \phi(\widehat{v_i^{t'}}) \tag{5.24}$$

$$s_j^* = \kappa_s * s_j \tag{5.25}$$

Where s_i is the postsynaptic spiketrain and V_i^* is the error between dendritic prediction and somatic rate and $h(u)$. The additional nonlinearity $h(u) = \frac{d}{du} ln \ \phi(u)$ is ommited in our model **TODO: should it though?**.

Antiderivatives:

$$\int_{-\infty}^x H(t) dt = t H(t) = max(0, t) \tag{5.26}$$

$$\tau_l = \frac{C_m}{g_L} = 10 \tag{5.27}$$

$$\tau_s = 3 \tag{5.28}$$

Writing membrane potential to history (happens at every update step of the postsynaptic neuron):

```
UrbanczikArchivingNode< urbanczik_parameters >::write_urbanczik_history(Time t
    , double V_W, int n_spikes, int comp)
{
  double V_W_star = ( ( E_L * g_L + V_W * g_D ) / ( g_D + g_L ) );
  double dPI = ( n_spikes - phi( V_W_star ) * Time::get_resolution().get_ms()
    )
      * h( V_W_star );
}
```

I interpret this as:

$$\int_{t_{ls}}^{T} dt' \ V_i^* = \int_{t_{ls}}^{T} dt' \ (s_i - \phi(V_i))h(V_i), \tag{5.29}$$

$$\int_{t_{ls}}^{T} dt' \ V_i^* = \sum_{t=t_{ls}}^{T} (s_i(t) - \phi(V_i^t)\Delta t)h(V_i^t) \tag{5.30}$$

$$\tag{5.31}$$

```
for (t = t_ls; t< T; t = t + delta_t)
{
    minus_delta_t = t_ls - t;
    minus_t_down = t - T;
    PI = ( kappa_l * exp( minus_delta_t / tau_L ) - kappa_s * exp(
    minus_delta_t / tau_s ) ) * V_star(t);
    PI_integral_ += PI;
    dPI_exp_integral += exp( minus_t_down / tau_Delta_ ) * PI;
}
// I_2 (t,T) = I_20(0,t) * exp(-(T-t)/tau) + I_2(t,T)
PI_exp_integral_ = (exp((t_ls-T)/tau_Delta_) * PI_exp_integral_ +
    dPI_exp_integral);
W_ji = PI_integral_ - PI_exp_integral_;
W_ji = init_weight_ + W_ji * 15.0 * C_m * tau_s * eta_ / ( g_L * ( tau_L -
    tau_s ) );

kappa_l = kappa_l * exp((t_ls - T)/tau_L) + 1.0;
kappa_s = kappa_s * exp((t_ls - T)/tau_s) + 1.0;

```

$$\int_{t_{ls}}^{T} dt' s_j^* = \tilde{\kappa}_L(t') * s_j - \tilde{\kappa}_s(t') * s_j \tag{5.32}$$

I_1 in the code is computed as a sum:

$$I_1(t, T) = \sum_{t'=t}^{T} \left(s_L^*(t') - s_s^*(t') \right) * V^*(t') \tag{5.33}$$

5.3   Dendritic leakage conductance

In order to match the dendritic potential of rate neurons in the spiking neuron model, a suitable leakage conductance for dendritic compartments was required. As described in Equation 2.20, a dendritic compartment evolves according to:

$$C_m^{dend} \dot{v}_j^{dend} = -g_l^{dend} \, v_j^{dend} + \sum_i W_{ji} \, \langle n_i \rangle \tag{5.34}$$

Under the assumption that the activation of all presynaptic neurons i remains static over time, we can replace the spontaneous activation $s_i(t)$ with the expected number of spikes per simulation step $\langle n_i \rangle = r_i \, \Delta t$ (cf Equation 2.18). Note that these values do not employ matrix notation, but concern individual neurons. Next, in order to find the convergence point of the ODE, we set the left side of the equation to 0 and to solve it:

$$0 = -g_l^{dend} \, v_j^{dend} + \sum_i W_{ji} \, r_i \, \Delta t \tag{5.35}$$

$$g_l^{dend} \, v_j^{dend} = W_{ji} \, r_i \, \Delta t \tag{5.36}$$

The desired dendritic potential of rate neurons is $v_j^{dend} = \sum_i W_{ji} \, r_i$, which occurs on both sides of the above equation. Assuming that our dendritic model fulfills this equality, both terms to drop out from the equation. Thus, the correct parametrization for the dendritic leakage conductance remains:

$$g_l^{dend} = \Delta t \tag{5.37}$$

It was shown experimentally that for hight spike frequencies, this parameterization leads to an exact match of dendritic potentials between the neuron models. It will therefore be assumed as the default throughout all experiments where spiking neurons are used.

In order to keep the NEST models as similar as possible, rate neurons evolve according

to the same dynamics. Like in the original implementation, dendrites of rate neurons are fully defined by their inputs at time t. This behaviour is acheived by setting the leakage conductance to 1 for all dendritic compartments. During network initialization, dendritic leakage conductances are set to either one of these values depending on the type of neuron model employed.

5.4 Plasticity in feedback connections

Within the present model, Pyramidal-to-pyramidal feedback weights evolve according to:

$$\dot{w}_l^{down} = \eta_l^{down} \ (\phi(u_l^P) - \phi(w_l^{down} r_{l+1}^P)) \ \phi(u_{l+1}^P)^T \tag{5.38}$$

The error term in this case differs slightly from the others, but could arguably still be implemented by biological neurons. An intuitive way to interpret the error term is as the difference between somatic activity and the activity of a distant apical compartment that is innervated only by superficial pyramidal neurons. Within the NEST implementation, this distal compartment leaks into the proximal apical compartment (v^{api}) with a conductance of $g^{api,dist} = 1$. The separation of pyramidal neuron apical dendrites into a proximal and a distal tree is well documented **TODO: cite**. A difference between plasticity mechanisms for synapses arriving at these two integration zones is plausible, although I was unable to find prior research supporting this type of plasticity **TODO: cite**. A more sophisticated model of the apical tree which resembles pyramidal neurons more closely could be a desirable extension to the model.

While the plasticity was successfully implemented in all variants of the model, it did not prove useful for training the networks during my tests. A strong indicator to the reason behind this is the fact, that the dendritic error for this rule is nonzero, even in the self-predicting state (cf. Figure 2.3). Making these connections non-plastic led to the best learning performance, and is therefore assumed as the default for all training simulations. This matches the previous implementations of this network too, which typically set learning rates of these connections to 0 with the exception of a few experiments employing steady-state approximations. Note that feedback information is transmitted through fixed weights in this case. Feedforward weights in turn learn to match these, meaning that the network effectively implements a type of Feedback alignment Lillicrap et al. (2014).

5.5 Presentation times and Latent Equilibrium

Exactly matching parameters and the training environment to those of existing implementations turned out to be a significant challenge. Particularly the way NEST handles signal transmissions made and exact numerical replication of results impossible, as discussed in Sec-
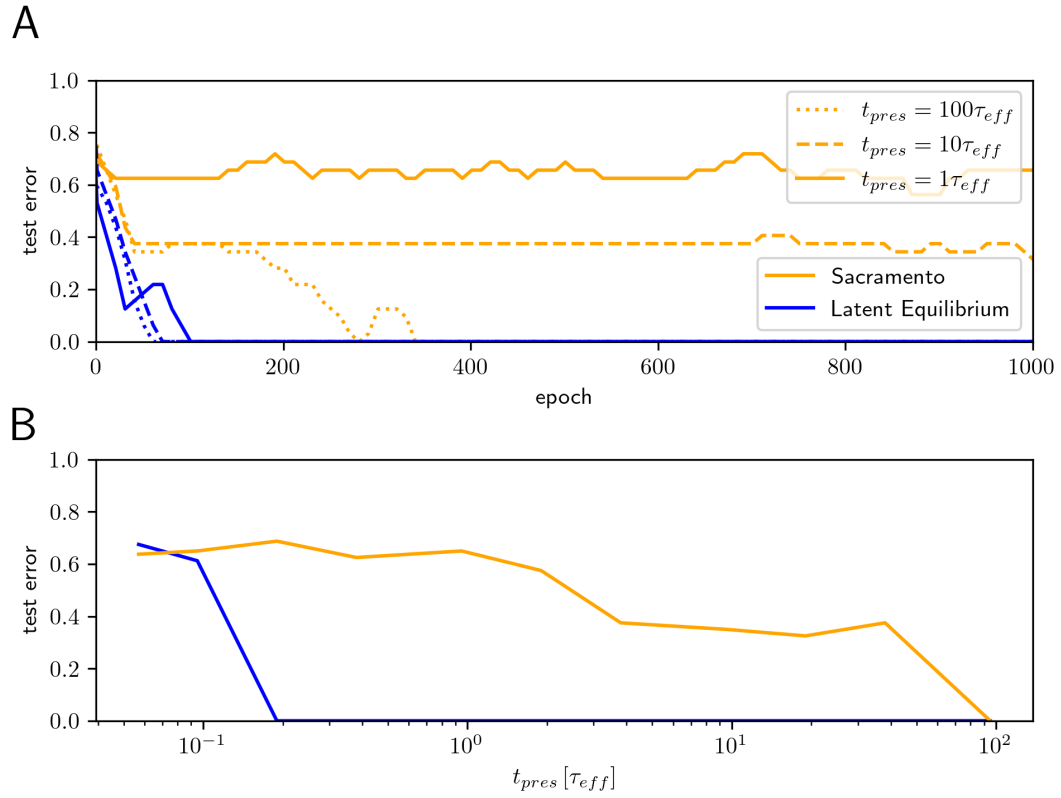
A

B

Figure 5.1: Replication of Figure 3.2 using a slightly modified version of the python code from Haider et al. (2021). Resulting performance matches the original results closely, showing that this version can serve as a baseline for comparing performance of the NEST implementation to the original results.

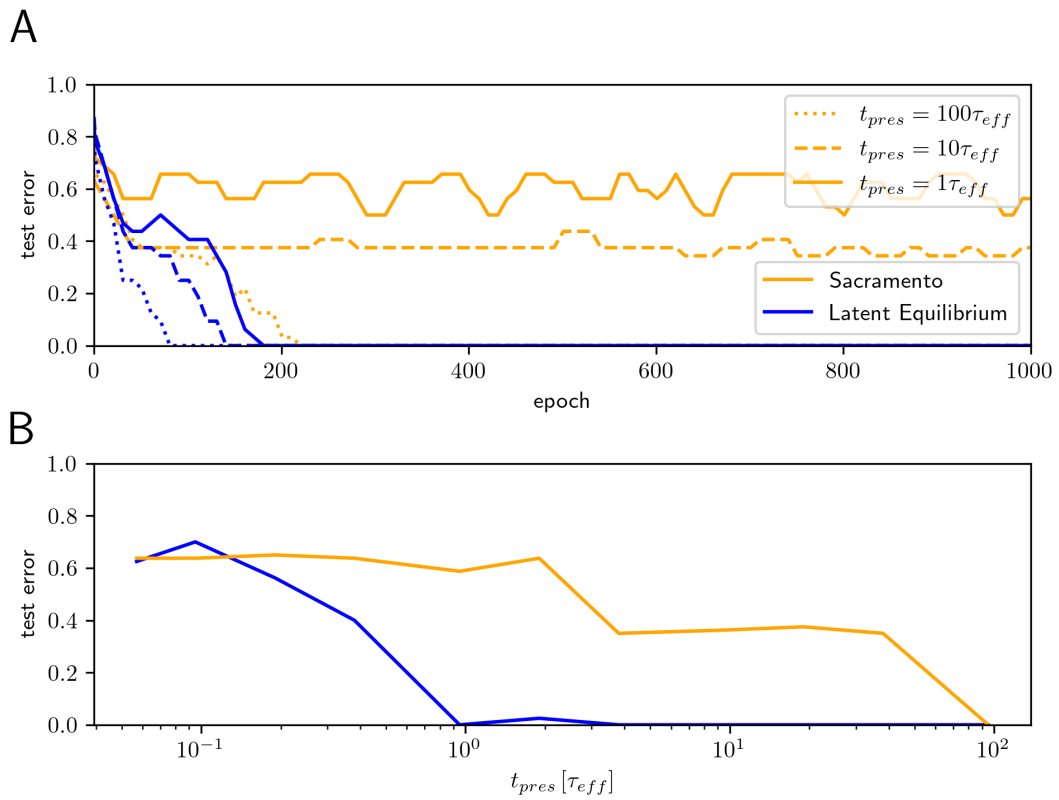tion **TODO: talk about timing differences**. In order to validate, that

Figure 5.2: Replication of Figure 3.2 using networks of rate neurons in the NEST simulator. A notable difference to the python implementation in Figure 5.1 is, that this version does not handle very low presentation times as well. This can likely be traced back to the synaptic delay enforced by NEST, which imposes an upper bound on network relaxation time. Besides that, performance of the two variants is very similar.

Chapter 6

additional notes and questions

6.1 Questions

- Is refractoryness interesting to us or more of a sidenote?

- Neuron dropout?

- How does one prove that the network is converged and will not diverge again.

- randomized/longer synaptic delays?

- As a follow up of dropout, maybe even neurogenesis?

- Should I look at delaying injection of the target activation?

- more ways in which this is biologically implausible?

- how interested are you in the code? reference it, explain it, or shut up?

6.2 TODOS

- In the torch implementation, there no persistence between timesteps at all. Input is fed into the network and processed feedforward and feedback. Output is read and weights (+biases) are updated. Rinse and repeat.

- to what extent should dendritic and somatic compartments decay?

- Can (should) we transfer the learned bias from the torch model?

- I can "cheat" the apical voltage constraint for self prediction by increasing apical leakage conductance. How does this influence my model?

- Is there some analytical approach to identifying why synaptic weights deviate from their intended targets?

- Show the limits of learning capability (i.e. how big of a network it can match)

- Test the network on a real-world dataset (mnist)

- prove/find literature on why the poisson process is a rate neuron in the limit.

- Does the network still learn when neurons have a refractory period?

- Comparison to other spiking backprops

- what can we learn from this? does it describe part of the brain

- talk about feedback plasticity

- Do the membrane capacitance experiments for basal dendrites aswell.

- redo the spike rate experiment, but investigate whether novel stimuli cause bursts.

- Reconsider title?

- replace cite with citep

6.3   Observations

- oversize networks fail more often. No idea why

- Different configurations for which synapses are plastic should be elaborated on.

6.4   Preliminary structural components

6.4.1   Synaptic delays

Where I will inspect the implications of synaptic delays inherent to the NEST simulations on the model and plasticity rule. In particular, I will look at the biological necessity for this type of delay and discuss why any model attempting to replicate neuronal processes must be resilient to these delays.

6.4.2   The relation between the pyramidal microcircuit and actual microcircuits

Where I can finally use the shit that has been on my whiteboard for half a year...

This will also serve as valuable insight into how plausible this microcircuit actually is, and might give some insight into possible model extensions.

6.4.3   Interneurons and their jobs

6.4.4   tpres

$t_{pres}10 - 50\tau$

Bibliography

Abbott, L. F. and Nelson, S. B. (2000). Synaptic plasticity: taming the beast. *Nature neuroscience*, 3(11):1178–1183.

Bartunov, S., Santoro, A., Richards, B., Marris, L., Hinton, G. E., and Lillicrap, T. (2018). Assessing the scalability of biologically-motivated deep learning algorithms and architectures. *Advances in neural information processing systems*, 31.

Bellec, G., Scherr, F., Hajek, E., Salaj, D., Legenstein, R., and Maass, W. (2019). Biologically inspired alternatives to backpropagation through time for learning in recurrent neural nets. *arXiv preprint arXiv:1901.09049*.

Bellec, G., Scherr, F., Subramoney, A., Hajek, E., Salaj, D., Legenstein, R., and Maass, W. (2020). A solution to the learning dilemma for recurrent networks of spiking neurons. *Nature communications*, 11(1):1–15.

Bengio, Y., Lee, D.-H., Bornschein, J., Mesnard, T., and Lin, Z. (2015). Towards biologically plausible deep learning. *arXiv preprint arXiv:1502.04156*.

Bengio, Y., Mesnard, T., Fischer, A., Zhang, S., and Wu, Y. (2017). Stdp-compatible approximation of backpropagation in an energy-based model. *Neural computation*, 29(3):555–577.

Brea, J. and Gerstner, W. (2016). Does computational neuroscience need new synaptic learning paradigms? *Current opinion in behavioral sciences*, 11:61–66.

Crick, F. (1989). The recent excitement about neural networks. *Nature*, 337(6203):129–132.

Davies, M., Srinivasa, N., Lin, T.-H., Chinya, G., Cao, Y., Choday, S. H., Dimou, G., Joshi, P., Imam, N., Jain, S., et al. (2018). Loihi: A neuromorphic manycore processor with on-chip learning. *Ieee Micro*, 38(1):82–99.

de Schepper, R., Deepu, R., Morales-Gregorio, A., Kitayama, I., Mitchell, J., Linssen, C., Enan, M., Eppler, J. M., Spreizer, S., Kamiji, N. L., et al. (2022). Nest 3.2. Technical report.

Eppler, J. M., Helias, M., Muller, E., Diesmann, M., and Gewaltig, M.-O. (2009). Pynest: a convenient interface to the nest simulator. *Frontiers in neuroinformatics*, 2:12.

Eyal, G., Verhoog, M. B., Testa-Silva, G., Deitcher, Y., Benavides-Piccione, R., DeFelipe, J., De Kock, C. P., Mansvelder, H. D., and Segev, I. (2018). Human cortical pyramidal neurons: from spines to spikes via models. *Frontiers in cellular neuroscience*, 12:181.

Gerstner, W. and Naud, R. (2009). How good are neuron models? *Science*, 326(5951):379–380.

Ginzburg, I. and Sompolinsky, H. (1994). Theory of correlations in stochastic neural networks. *Physical review E*, 50(4):3171.

Grossberg, S. (1987). Competitive learning: From interactive activation to adaptive resonance. *Cognitive science*, 11(1):23–63.

Guerguiev, J., Lillicrap, T. P., and Richards, B. A. (2017). Towards deep learning with segregated dendrites. *ELife*, 6:e22901.

Haider, P., Ellenberger, B., Kriener, L., Jordan, J., Senn, W., and Petrovici, M. A. (2021). Latent equilibrium: A unified learning theory for arbitrarily fast computation with arbitrarily slow neurons. *Advances in Neural Information Processing Systems*, 34:17839–17851.

Hines, M. L. and Carnevale, N. T. (1997). The neuron simulation environment. *Neural computation*, 9(6):1179–1209.

Izhikevich, E. M. (2007). Solving the distal reward problem through linkage of stdp and dopamine signaling. *Cerebral cortex*, 17(10):2443–2452.

Kawaguchi, Y. (2001). Distinct firing patterns of neuronal subtypes in cortical synchronized activities. *Journal of Neuroscience*, 21(18):7261–7272.

Liao, Q., Leibo, J., and Poggio, T. (2016). How important is weight symmetry in backpropagation? In *Proceedings of the AAAI Conference on Artificial Intelligence*, volume 30.

Lillicrap, T. P., Cownden, D., Tweed, D. B., and Akerman, C. J. (2014). Random feedback weights support learning in deep neural networks. *arXiv preprint arXiv:1411.0247*.

Magee, J. C. and Grienberger, C. (2020). Synaptic plasticity forms and functions. *Annual review of neuroscience*, 43:95–117.

Mancilla, J. G., Lewis, T. J., Pinto, D. J., Rinzel, J., and Connors, B. W. (2007). Synchronization of electrically coupled pairs of inhibitory interneurons in neocortex. *Journal of Neuroscience*, 27(8):2058–2073.

Mazzoni, P., Andersen, R. A., and Jordan, M. I. (1991). A more biologically plausible learning rule for neural networks. *Proceedings of the National Academy of Sciences*, 88(10):4433–4437.

McClelland, J. L., McNaughton, B. L., and O'Reilly, R. C. (1995). Why there are complementary learning systems in the hippocampus and neocortex: insights from the successes and failures of connectionist models of learning and memory. *Psychological review*, 102(3):419.

McCormick, D. A., Connors, B. W., Lighthall, J. W., and Prince, D. A. (1985). Comparative electrophysiology of pyramidal and sparsely spiny stellate neurons of the neocortex. *Journal of neurophysiology*, 54(4):782–806.

Millidge, B., Tschantz, A., Seth, A. K., and Buckley, C. L. (2020). Activation relaxation: A local dynamical approximation to backpropagation in the brain. *arXiv preprint arXiv:2009.05359*.

O'Reilly, R. C. (1996). Biologically plausible error-driven learning using local activation differences: The generalized recirculation algorithm. *Neural computation*, 8(5):895–938.

Potjans, T. C. and Diesmann, M. (2014). The cell-type specific cortical microcircuit: relating structure and activity in a full-scale spiking network model. *Cerebral cortex*, 24(3):785–806.

Rao, R. P. and Ballard, D. H. (1999). Predictive coding in the visual cortex: a functional interpretation of some extra-classical receptive-field effects. *Nature neuroscience*, 2(1):79–87.

Roelfsema, P. R. and Holtmaat, A. (2018). Control of synaptic plasticity in deep cortical networks. *Nature Reviews Neuroscience*, 19(3):166–180.

Sacramento, J., Ponte Costa, R., Bengio, Y., and Senn, W. (2018). Dendritic cortical microcircuits approximate the backpropagation algorithm. *Advances in neural information processing systems*, 31.

Seung, H. S. (2003). Learning in spiking neural networks by reinforcement of stochastic synaptic transmission. *Neuron*, 40(6):1063–1073.

Sjostrom, P. J., Rancz, E. A., Roth, A., and Hausser, M. (2008). Dendritic excitability and synaptic plasticity. *Physiological reviews*, 88(2):769–840.

Stapmanns, J., Hahne, J., Helias, M., Bolten, M., Diesmann, M., and Dahmen, D. (2021). Event-based update of synapses in voltage-based learning rules. *Frontiers in neuroinformatics*, page 15.

Urbanczik, R. and Senn, W. (2014). Learning by the dendritic prediction of somatic spiking. *Neuron*, 81(3):521–528.

Van Albada, S. J., Rowley, A. G., Senk, J., Hopkins, M., Schmidt, M., Stokes, A. B., Lester, D. R., Diesmann, M., and Furber, S. B. (2018). Performance comparison of the digital neuromorphic hardware spinnaker and the neural network simulation software nest for a full-scale cortical microcircuit model. *Frontiers in neuroscience*, 12:291.

Vaughn, M. J. and Haas, J. S. (2022). On the diverse functions of electrical synapses. *Frontiers in Cellular Neuroscience*, 16.

Vezoli, J., Falchier, A., Jouve, B., Knoblauch, K., Young, M., and Kennedy, H. (2004). Quantitative analysis of connectivity in the visual cortex: extracting function from structure. *The Neuroscientist*, 10(5):476–482.

Werfel, J., Xie, X., and Seung, H. (2003). Learning curves for stochastic gradient descent in linear feedforward networks. *Advances in neural information processing systems*, 16.

Whittington, J. C. and Bogacz, R. (2017). An approximation of the error backpropagation algorithm in a predictive coding network with local hebbian synaptic plasticity. *Neural computation*, 29(5):1229–1262.

Whittington, J. C. and Bogacz, R. (2019). Theories of error back-propagation in the brain. *Trends in cognitive sciences*, 23(3):235–250.

Yamins, D. L. and DiCarlo, J. J. (2016). Using goal-driven deep learning models to understand sensory cortex. *Nature neuroscience*, 19(3):356–365.